Subsurface Imaging with Reverse Vertical Seismic Profiles

Mary Krasovec, Richard Coates, M. Nafi Toksöz

Abstract

A novel imaging process, referred to as vector image isochron (VII) migration, is specifically designed to reduce artifacts caused by arrays with limited apertures. By examining the assumptions behind generalized Radon transform (GRT) migration, a new approach is found which identifies and suppresses array artifacts, based on the array geometry and the migration earth model.

The new method works in four steps: 1) The conventional image is broken down according to the orientation of imaged planes within the image space, forming a *vector image* of the earth; 2) the earth model and the geometry of the arrays are used to derive *vector image isochrons*, which define the shape of reflection events in the vector image space; 3) the vector image is transformed by summing along the isochrons so that it depends on subsurface location and *reflector* orientation, rather than *imaged plane* orientation. This process is referred to as vector image isochron (VII) transformation; and 4) the transformed vector image is collapsed to a scalar image by summing over reflector orientations.

The VII imaging method is derived in both 2D and 3D with the assumption that at least one of the arrays, source or receiver, is oriented horizontally. The surface array can have any distribution along the surface. The other array can have any orientation, although in this paper it will be assumed to be either another surface array or a vertically oriented downhole array. Downhole surveys in deviated wells, or in multiple wells, can be imaged with VII migration, at the likely cost of more computation time.

The VII imaging method is tested on field data acquired in 1998 by MIT and several industry partners. The dataset is a 3D reverse vertical seismic profile (RVSP) over a hydrocarbon-bearing pinnacle reef in the northern Michigan reef trend. The survey exhibited two features of note: 1) A new, strong, downhole vertical vibrator, and 2) a random distribution of surface receiver locations. Due to adverse conditions, a large portion of the surface spread had to be abandoned. The reduced spatial coverage presents a challenge to the new migration method, but also limits the extent of the migrated image, precluding an evaluation of the effectiveness of the random receiver spread.

The limited nature of the receiver array also causes artifacts in the image which resemble migration "smiles". These are partially suppressed by limiting the dip aperture of the migration, but this also limits the reflector dips that can be imaged. The new VII imaging scheme, on the other hand, removes the artifacts without diminishing dipping reflectors. The VII images show more continuity along reflectors than images made with the conventional method.

1 Introduction

Many geophysical applications rely on high resolution seismic imaging of the earth's interior: petroleum exploration, development of geothermal resources, earthquake location, and near surface mapping of pollutants, to name a few. The portfolio of tools available for such characterization of the near surface has been recently expanding, especially within the petroleum industry where imaging goals have shifted from the identification of new targets to the development of known reservoirs.

In order to increase resolution, it is desirable to put either the source array or the receiver array in a wellbore. The decreased distance traveled by the seismic energy means less attenuation of high frequencies resulting in more detailed images. On the down side, these images tend to cover only a small portion of the desired target. The location of illuminated areas depends on the structure of the subsurface, and images produced with borehole seismic data tend to have artifacts caused by limited illumination of the borehole seismic array. We proposes a method of recognizing and minimizing array artifacts by accounting for the survey geometry. The new method is applied to a reverse vertical seismic profile (RVSP) attained at MIT's Michigan Test Site.

The proposed imaging method is in principle GRT (generalized Radon transform) migration, with additional steps taken to analyze the geometry of the source and receiver arrays, based on the earth model and information in the data. Each point in the image is viewed as a sum of contributions from various imaged planes and scattering angles, and the final image is formed using knowledge of the orientation of the reflectors to improve the image quality, minimizing array artifacts.

To date, most published VSP imaging case studies have used migration techniques which were originally developed for data collected with surface seismic arrays, such as methods used by Stolt (1978) and Gazdag (1978). Some of the assumptions made in the initial derivations of these migration methods do not apply to borehole seismic data.

The first section of this paper will show that surface seismic data migration assumes that the ray coverage of each subsurface point is symmetric: for each ray that images a plane dipping to the left, another ray will image a plane dipping the same angle to the right. This is not the case with borehole seismic data.

A drawback of the new method is a loss of image resolution. In the derivation of the new method, some expressions are derived with the assumption of straight rays, the introduces some error which leads to the loss of resolution.

2 The new migration method

The new method is described in four parts. First, GRT migration is used to form an image of the earth which depends not only on subsurface location but also on the orientation of the imaged plane. This image is referred to as a *vector image*.

Second, *vector image isochrons*, which define the shape of reflection events in the vector image space, are derived. Explicit derivations of the isochrons depend on the array geometry, and are detailed in the Appendices.

Next, the vector image is transformed by summing it along the isochrons, focusing reflected energy to the depth and plane from which it is reflected. The transformed image therefore depends on subsurface location and *reflector* orientation, rather than on *imaged plane* orientation. This process is referred to as vector image isochron (VII) transformation.

Finally, the transformed vector image is collapsed to a scalar image by summing over reflector orientations.

2.1 The vector image migration integral

Let $\mathbf{x}$ be a point in the image grid, and let a plane P passing through $\mathbf{x}$ be described by its upward pointing normal $\mathbf{p}$. Seismic energy is incident on P at $\mathbf{x}$, and reflects according to Snell's law. The incident and reflected rays are described by normals $\mathbf{s}$ and $\mathbf{r}$, respectively, which both point upward, away from the image point $\mathbf{x}$.

Two sets of angles will be used to describe $\mathbf{s}$ and $\mathbf{r}$. First, a vector angle $\phi = [\phi_a, \phi_d]$ describes the imaged plane normal $\mathbf{p}$, as shown in Figure 1. ϕ_a is an azimuth of $\mathbf{p}$ measured relative to the +x axis and ϕ_d is the angle $\mathbf{p}$ makes with the z axis.

Second, the vector $\iota = [\iota_a, \iota_d]$ describes the angle at which energy is reflected from the imaged plane, as shown in Figure 2. ι_a is the azimuth of $\mathbf{r}$ measured relative to the azimuth of $\mathbf{p}$, and ι_d is the angle $\mathbf{r}$ makes with $\mathbf{p}$. ι_a is in the range [0^o, 180^o), and ι_d is in (-90^o, 90^o).

Given some earth model, i.e. the migration velocity model, the source and receiver locations can be found by ray tracing in the directions defined by $\mathbf{s}$ and $\mathbf{r}$. For a plane $(\mathbf{x}, \phi)$, each value of ι describes a unique source receiver pair, and a unique traveltime.

$$\mathbf{x_s} \equiv \mathbf{x_s}(\mathbf{x}, \phi, \iota) \tag{1}$$

$$\mathbf{x_r} \equiv \mathbf{x_r}(\mathbf{x}, \phi, \iota) \tag{2}$$

$$t_{mig} \equiv t_{mig}(\mathbf{x}, \phi, \iota) \tag{3}$$

With this geometry, a migration process which forms a vector image $V(\mathbf{x}, \phi)$ can be expressed as a sum over the incidence angle ι. In an idealized experiment where the seismic displacement is known at every

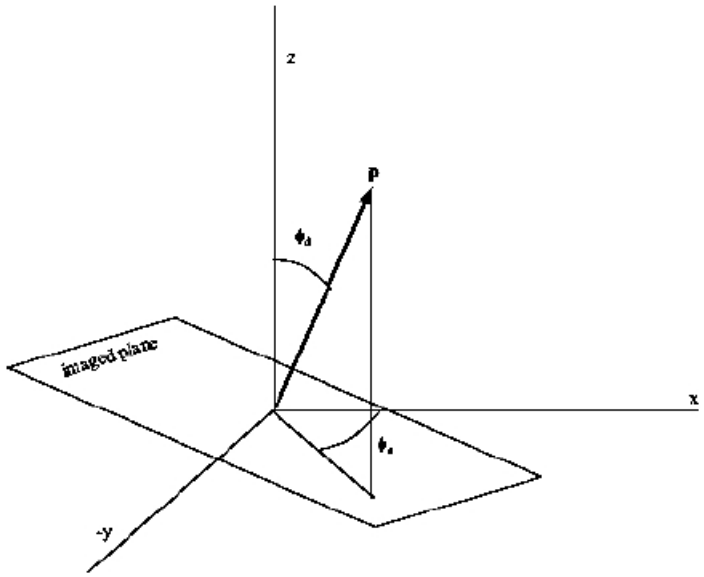

Figure 1: Geometry of the imaged plane. Angles ϕ_a and ϕ_d describe the orientation of $\mathbf{p}$, the normal to the imaged plane.

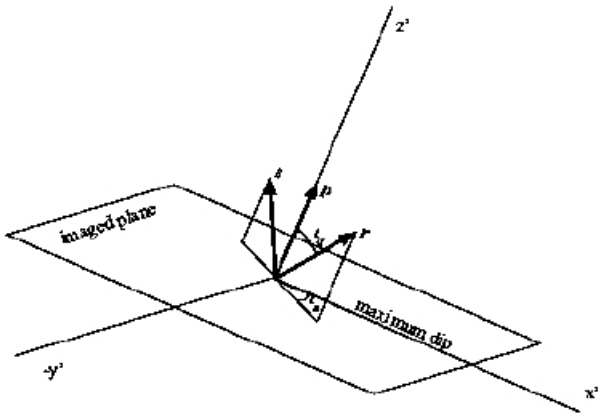

Figure 2: Prime coordinate system in which the reflector is horizontal. **p** is the image plane normal, and **s** and **r** are the normals to the incident and reflected rays. Angles ι_a and ι_d describe how the energy is incident on the plane.

point along the source and receiver arrays, the summation can be written as an integral:

$$V(\mathbf{x}, \phi) = \int c_{mig} u(\mathbf{x_s}, \mathbf{x_r}, t_{mig}) d\iota \tag{4}$$

where $u(\mathbf{x_s}, \mathbf{x_r}, t_{mig})$ represents the displacement measured at the time t_{mig} with the source and receiver at the points x_s and x_r. The weighting factor c_{mig} corrects for path length differences, wavefront spreading, and reflection amplitudes.

2.2 Isochrons in the vector image

The impulse response of the migration integral in Equation 4 is found by letting the seismic displacement measured by a receiver at $\mathbf{x_r}$ due to a source at $\mathbf{x_s}$ be a delta function. If A_{sr} and t_{sr} are the amplitude and traveltime along a specularly reflected ray, the measured displacement is:

$$u(x_s, x_r, t_{sr}) = A_{sr}\delta(t - t_{sr}). \tag{5}$$

The traveltime t_{sr} depends on the source and receiver positions and the earth model. If the ray corresponding to this traveltime reflected at a point $\mathbf{x_{ref}}$ on a reflector which, at point $\mathbf{x_{ref}}$, has orientation angle θ, then

$$t_{sr} \equiv t_{sr}(\mathbf{x_s}, \mathbf{x_r}, \mathbf{x_{ref}}, \theta). \tag{6}$$

Given the data in Equation 5, Equation 4 becomes:

$$V(\mathbf{x}, \phi) = \int c_{mig} A_{sr} \delta(t_{mig} - t_{sr}) d\iota \tag{7}$$

and is nonzero only when

$$t_{mig}(\mathbf{x}, \phi, \iota) = t_{sr}(\mathbf{x_s}, \mathbf{x_r}, \mathbf{x_{ref}}, \theta). \tag{8}$$

The geometry of this equality is shown in Figure 3. The details are discussed further in Section 3.1 and in Appendix A.

Since $\mathbf{x_s}$ and $\mathbf{x_r}$ can be described as in Equation 1, the equality 8 leads to a relation between $\mathbf{x}$, ϕ, and ι for a given reflector $\mathbf{x_{ref}}$, θ. This relation describes *vector image isochron* surfaces; for each value of ι, these surfaces are parameterized as functions of the imaged plane orientation ϕ and incidence angle ι_d:

$$\mathbf{x_{iso}} \equiv \mathbf{x_{iso}}(\phi, \iota; x_{ref}, \theta). \tag{9}$$

Since the isochrons depend on ray paths, they cannot be explicitly derived for a general earth model. They also rely on different assumptions for borehole seismic arrays than for surface seismic arrays. Appendices A and B derive vector image isochrons for surface seismic and borehole seismic arrays given two assumptions: (1) a constant velocity earth, and (2) linear or, in 3D, planar reflectors.

2.3 Transforming the vector image

The migration process in Equation 4 puts reflected energy along curves called vector image isochrons (Equation 9).

The vector image $V(\mathbf{x}, \phi)$ can be transformed by summing along isochrons. The transformed image $V'(\mathbf{x}, \theta)$ is:

$$\begin{aligned} V'(\mathbf{x_i}, \theta) &= \int V(\mathbf{x}, \phi)\delta(x - \mathbf{x_{iso}}(\phi; \mathbf{x_{ref}}, \theta) d\phi \\ &= \int V(\mathbf{x_{iso}}(\phi; \mathbf{x_{ref}}, \theta), \phi)) d\phi. \end{aligned} \tag{10}$$

This transform will be referred to as the vector image isochron (VII) transform. The transformed image can be thought of as a function of reflector orientation, whereas the untransformed vector image was a function of the imaged plane. Examples in later sections will illustrate the difference.

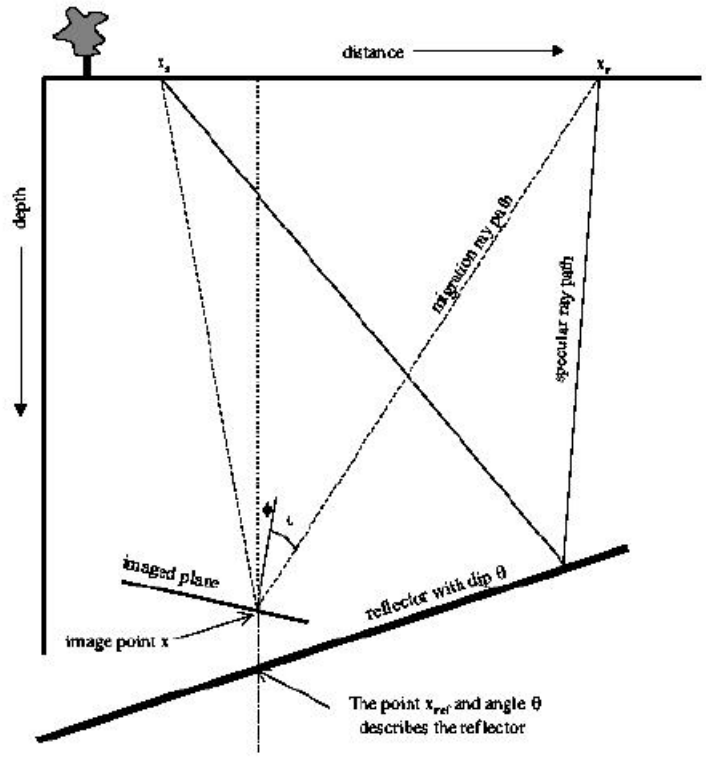

Figure 3: Principle used to derive the vector image isochrons (see Section A.1 for discussion).

2.4 Summation to a scalar image

To form a final scalar image, the transformed vector image is summed along reflector orientations:

$$I(\mathbf{x_{ref}}) = \int V'(\mathbf{x_{ref}}, \theta) d\theta. \tag{11}$$

3 Synthetic Data Examples

Detailed derivations of the isochrons can be found in the appendices. The results are found explicitly for surface seismic arrays, and numerically for borehole seismic arrays. The isochrons are described by fixing the x and y coordinates of the image point and letting z_{iso} be the depth of the isochron as a function of the imaged plane orientation angle(s) ϕ, the reflector depth at the image location z_{ref} and reflector orientation angle(s) θ.

3.1 Surface seismic isochrons in 2D

For surface seismics, the isochron depends on ι_d, the incidence angle at the imaged plane. In 2D, $\phi_a = \theta_a = \iota_a = 0$, and the isochron is:

$$\frac{z_{iso}}{z_{ref}} = \frac{\cos\theta_d(\sin\theta_d \sin\phi_d \cos\phi_d \pm \cos\iota_d \sqrt{\cos{\phi_d}^2 - \cos{\theta_d}^2 \sin{\iota_d}^2}}{\cos{\theta_d}^2 \cos{\iota_d}^2 + \sin{\theta_d}^2 \cos{\phi_d}^2}. \tag{12}$$

In the special case of a flat reflector, $\theta_d = 0$, and Equation 12 describes ellipses in $[z_{iso}, \sin\phi_d]$ space for each value of ι_d:

$$\left(\frac{z_{iso}}{z_{ref}}\right)^2 + \left(\frac{\sin\phi_d}{\cos\iota_d}\right)^2 = 1 \tag{13}$$

Figure 4 shows an image made with synthetic data for a reflector dipping at 20^o. Isochrons for several values of the incidence angle ι_d are plotted over the image. Because the reflector is dipping, the contours of ι_d are not ellipses. The more steeply the reflector dips, the further the contours are from ellipses, in more than just shape. In Figure 4, the peak energy is at the point $z/z_{ref} = 1$, $\phi_d = 20^o$, but the curve is slightly asymmetric in intensity as well as shape. The left branch of the curve, with negative ϕ_d, is slightly brighter and broader than the right branch.

To better understand Figure 4, recall that the migration raypath scattering angles ι_d are those for which the integrand in Equation 7 is nonzero, and the location of the contours shows the part of the image which receives some energy contribution from the dataset in Equation 5. The more closely the contours are spaced, the more energy that part of the image will have. The point where $z = z_{ref}$ and $\theta_d = 20^o$ corresponds to the location of the actual reflector. All contours overlap there, meaning that this point should have the most energy in the image.

All other points that lie on isochrons do not correspond to reflectors in the earth, but will still have some energy in the image. Theoretically, all points within the $\iota_d = 0$ ellipse will receive some contribution from the migration integral. Realistically, seismic surveys are not designed to sample large incidence angles. Reflection amplitudes become critical, usually at about 30^o. Also, large scattering angles tend to involve long ray paths, becoming increasingly difficult to measure. For this reason, as well as due to the spacing of the ι_d contours, most energy in the image is expected to lie near the $\iota_d = 0$ ellipse.

Since the energy is located along the $\iota_d = 0$ contour, only this contour is used in the surface seismic transform. Figure 5 shows the VII transform of the 2D surface seismic vector image in Figure 4. The energy has been focused to the point corresponding to the reflector.

3.2 Surface seismic isochrons in 3D

The 2D example showed that the energy of reflected events in the surface seismic vector image lies predominantly along the $\iota_d = 0$ contour. It is possible to make contours in 3D for any value of ι_d, but it isn't

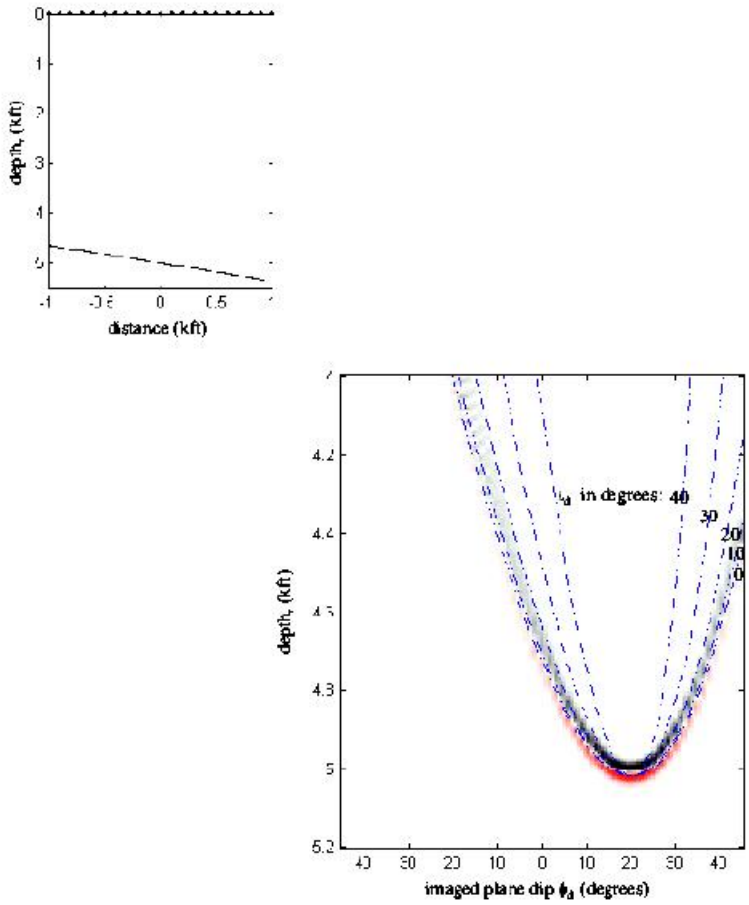

Figure 4: Image made with synthetic 2D surface seismic data for a reflector dipping at 20^o, with contours of the migration incidence angle ι_d.

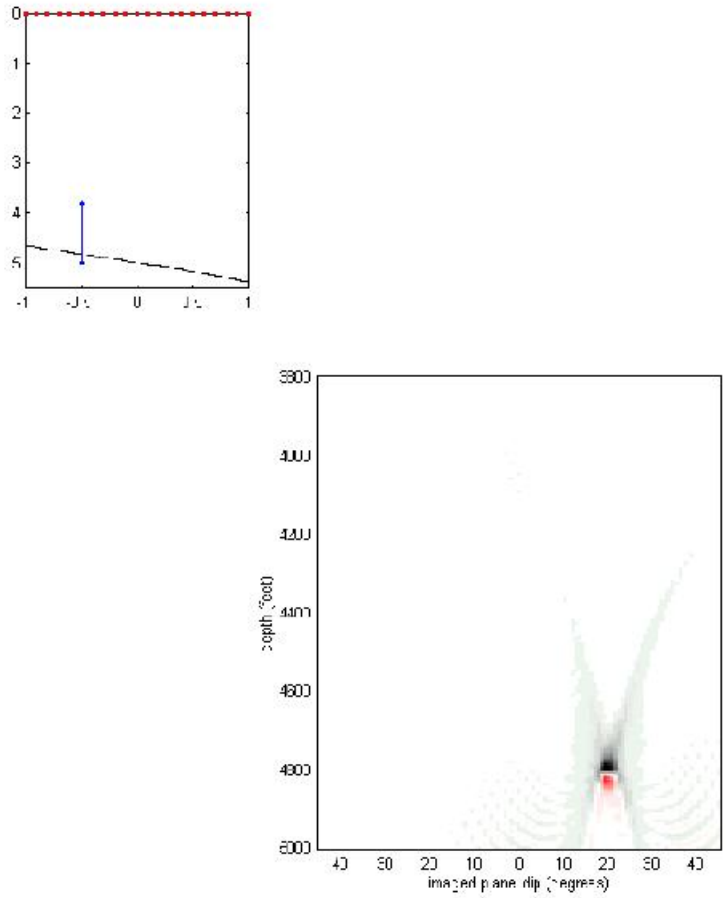

Figure 5: Transform of the 2D surface seismic image in Figure 4.

necessary, and much troublesome algebra can be avoided by setting $\iota_d = 0$ initially. Therefore, $\mathbf{s}$ and $\mathbf{r}$ are equal to $\mathbf{p}$ and the source and receiver have the same location $\mathbf{x_s}$.

In 3D, the reflector is described by its depth z_{ref} at the image point and the orientation of its normal, a two valued angle $\theta = [\theta_a, \theta_d]$. The imaged plane is similarly described by a two valued angle $\phi = [\phi_a, \phi_d]$. The isochron is:

$$\frac{z_{iso}}{z_{ref}} = \frac{-\cos\theta_d \cos\phi_d}{1 + \sin\phi_d \sin\theta_d(\cos\phi_a \cos\theta_a + \sin\phi_a \sin\theta_a)} \tag{14}$$

3.3 Borehole seismic array isochrons in 2D

A different approach is needed to map isochrons in borehole seismic vector images, since the source array has a fixed (x, y) location, but varies in depth. The approach taken here is to fix the source depth and calculate the isochrons one shot depth at a time. (The consequences of this assumption will be discussed in Section 3.6.) Since the isochrons are mapped one shot depth at a time, there is only one raypath which illuminates each image point and plane, as illustrated in Figure 6. The incidence angle ι will not be an independent variable as it was in the case of surface seismic arrays.

Another difference between surface array and borehole array isochrons, caused by the fixed (x, y) location of the source, is that the shape of the isochrons will be different at different image (x, y) locations.

The isochrons for borehole seismics in both 2D and 3D are found numerically, as described in the appendices.

Figure 7 shows a 2D borehole seismic image and its isochron according to Equation B-6. The asymmetry of the image is caused by the array. The cube in the upper left shows the dipping reflector, the shot location, and the line of surface receivers. The image is over the range of depths shown as a vertical line. Many planes are not imaged by the array; these are the positive dips and the large negative dips, where the vector image is blank.

Figure 8 shows the VII transform of the 2D borehole seismic image in Figure 7. The energy has been focused to the proper reflector location, although there is a "tail" to one side. When the transformed vector image is summed into the final spatial image, which is a sum horizontally across the image in Figure 8, energy in this tail will cancel out.

3.4 Borehole seismic array isochrons in 3D

Figure 9 shows a vector image from a 3D borehole seismic array and a single reflector. The actual reflector has a 20^o dip at an azimuth of 0^o.

Figure 10 shows the VII transform of the 3D borehole seismic image in Figure 9. The energy has been focused into the proper depth, dip and azimuth of the reflector, which had a dip of 10^o at an azimuth of 0^o.

3.5 Multiple Reflectors

Figure 11 shows a borehole seismic array and a 5 layer synthetic model. The model has five reflectors, and the two dipping reflectors have dips of 5^o and 15^o. In keeping with the final goal of this study, the sources are located in the well and the receivers on the surface, although for this simple synthetic example the source and receiver positions are interchangeable.

Figure 12 shows the result of wide aperture 45^o Kirchhoff migration of the synthetic RVSP data. Note that there are artifacts in even the flat reflectors. In addition, uneven illumination leads to variable amplitudes along the reflectors. Figure 13 shows a limited aperture image made with the RVSP data, with the maximum aperture of 20^o. The aperture limitation reduces the artifacts and slightly evens the reflector brightness, but also causes a loss of amplitude along the most steeply dipping reflector. The vector image at the x=0 location, right beneath the well, is shown in Figure 14. It transforms as in Figure 15; the final scalar image is shown in Figure 16. The VII method has removed the artifacts without losing the dipping reflector.

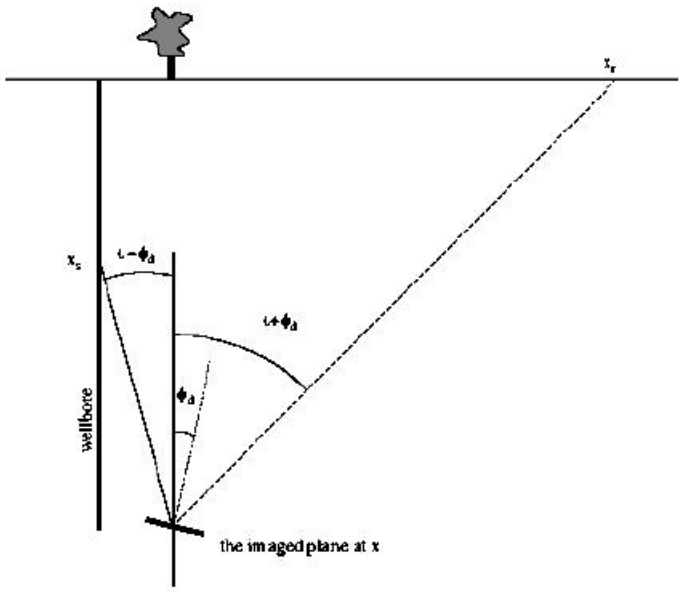

Figure 6: Geometry for borehole seismics. Source location is fixed, so that each imaged point and plane is imaged by a single receiver.

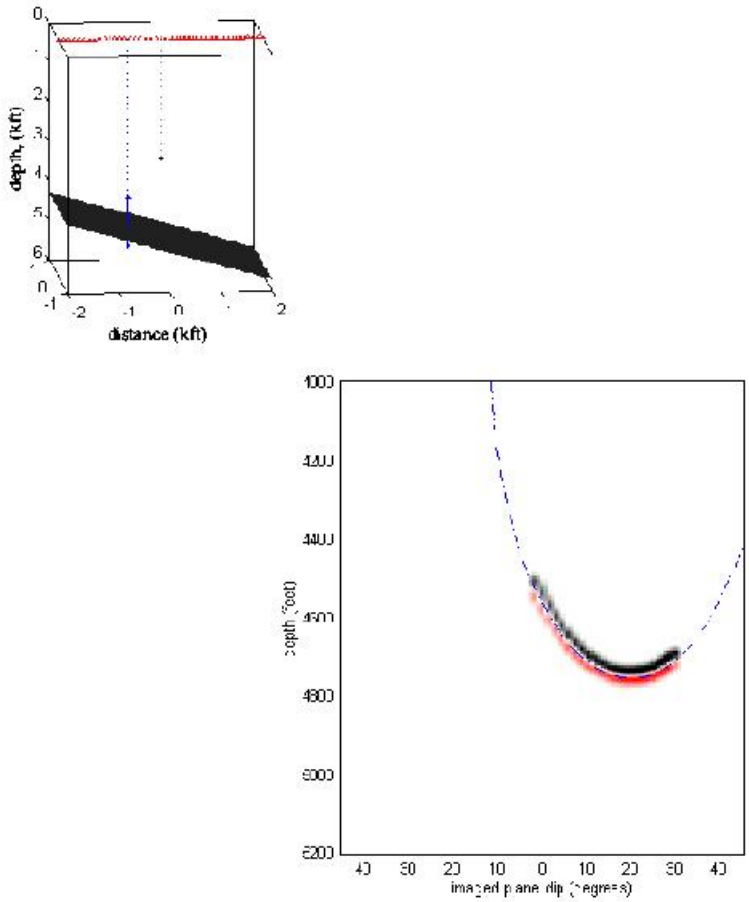

Figure 7: Vector image from a 2D single shot synthetic borehole seismic survey. The overlain isochron is the solution to Equation 12, found numerically.

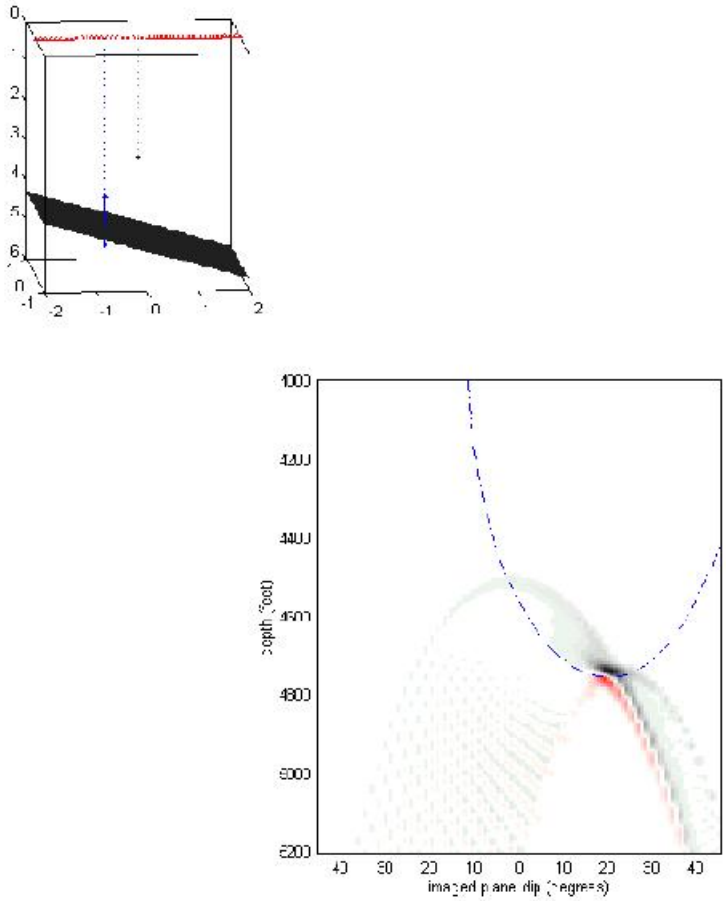

Figure 8: Transform of the 2D borehole seismic image in Figure 7.

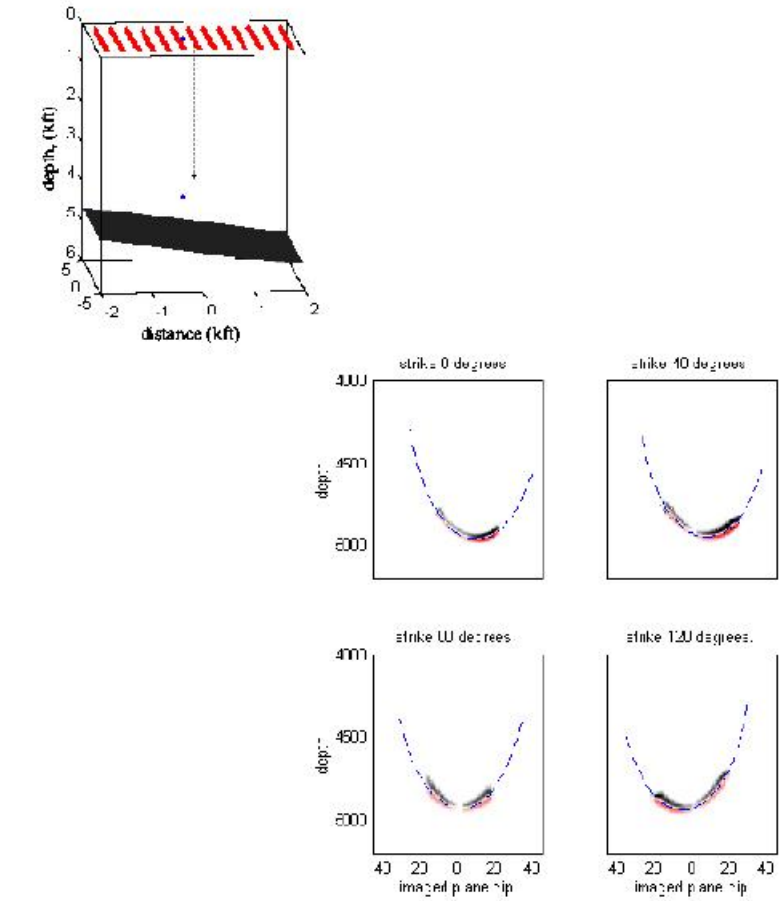

Figure 9: Vector image from a single shot synthetic 3D borehole seismic data; the dashed curves are vector image isochrons. The image x, y location is offset 200 feet (60 meters) from the shots in the well. The actual reflector has a dip of 10^oat a 0^o azimuth.

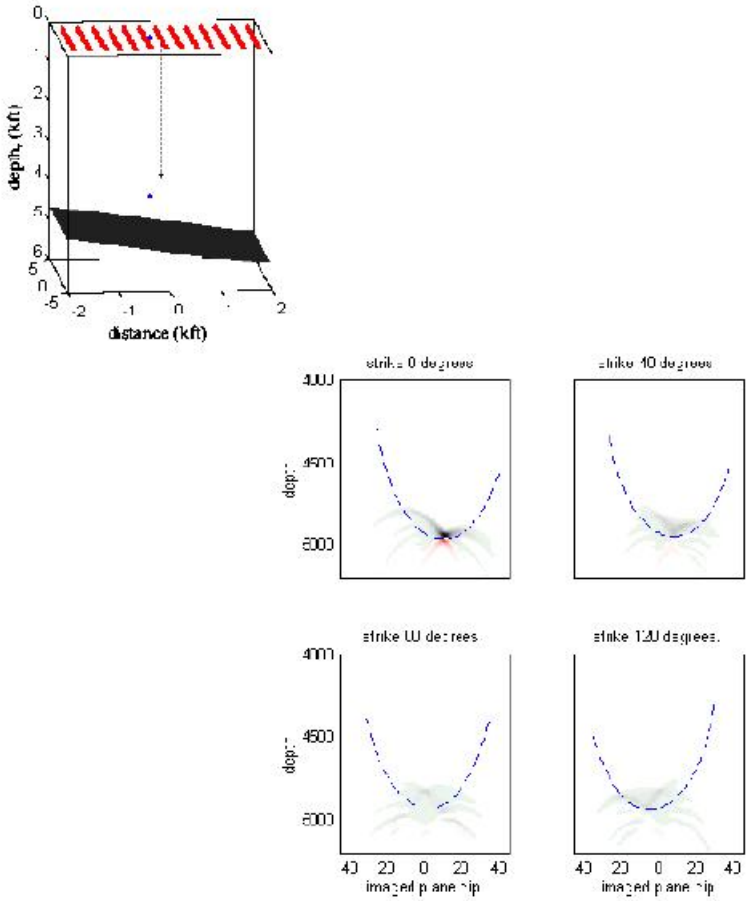

Figure 10: Transform of the 3D borehole seismic image in Figure 9.

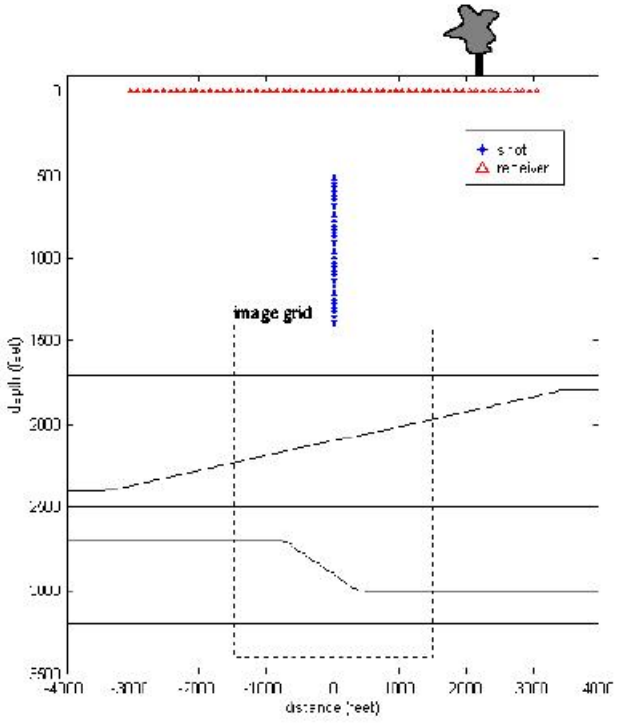

Figure 11: Geometry of the synthetic RVSP study.

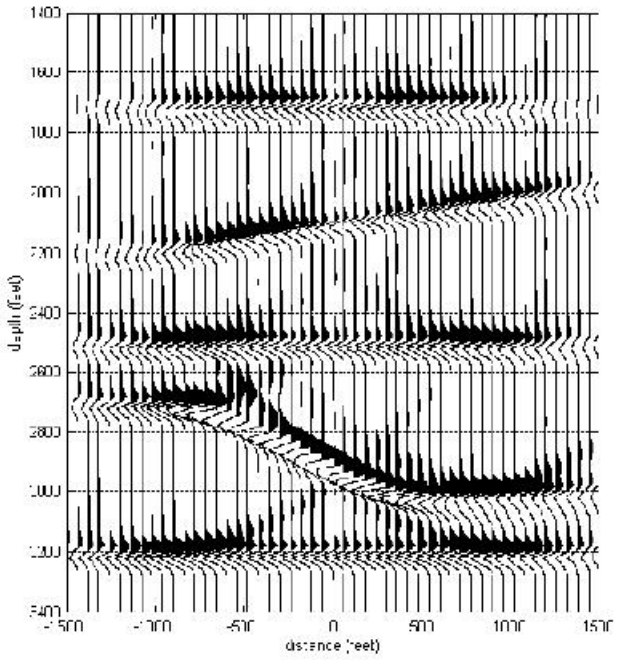

Figure 12: Wide aperture (45^o) RVSP imaging result. The triplication causes an artifact, but there are also artifacts in even the flat reflectors caused by the uneven coverage of the array.

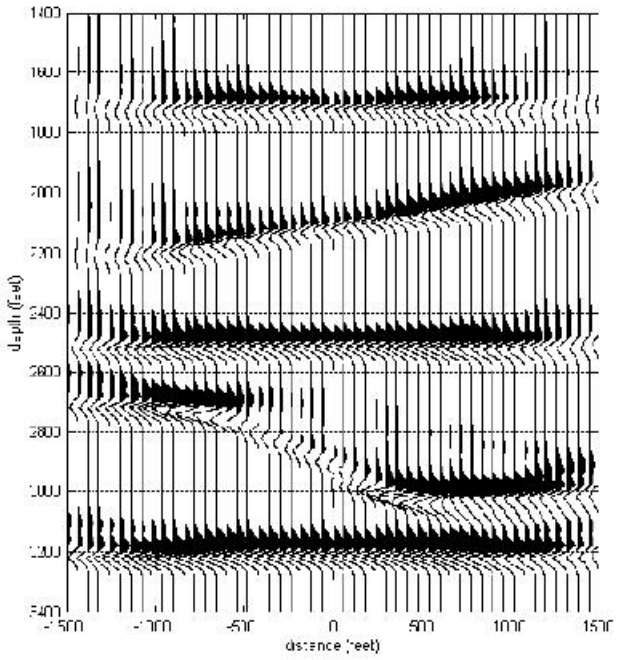

Figure 13: Limited aperture RVSP imaging result, with an aperture of $\pm 15^o$. The artifacts are reduced and amplitudes evened out somewhat, but at the cost of loss of brightness on the problematic fourth reflector.

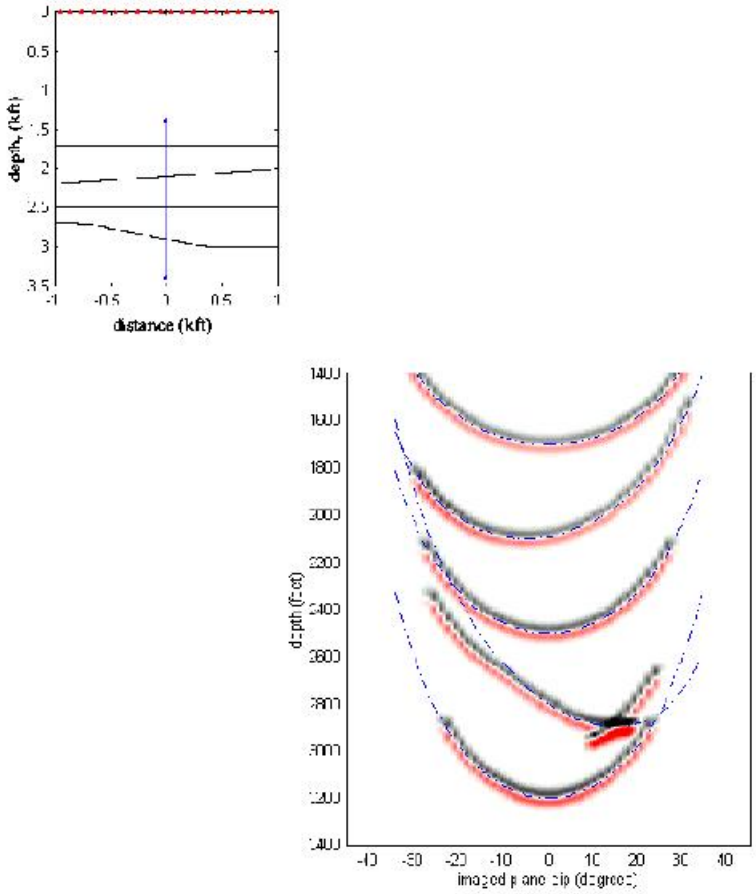

Figure 14: Vector image of the 5 reflector synthetic example.

3.6 Multiple shot depths

Figure 17 shows a 2D image made with a sparse array of borehole sources. The contribution of each shot to the image can be seen, and fits isochrons calculated for the various shot depths. The image point is fairly close to the source array, so there is a noticable difference between the isochrons for the different shot depths.

The ideal way to image in this case would be to migrate, transform, and sum one shot location at a time, then add the resulting images. However, since most of the energy lies where the isochrons for the various shot depths are close together; transforming once for a midlevel shot depth may be sufficent in many cases.

Transforming one shot at a time would be most necessary when the image location is far to the side of the well and near the shots in depth, as the isochrons in these cases are more spread. This can be tested by making an isochron plot before imaging.

4 Field data imaging results

This section presents field data images made with the reverse VSP data collected in a 1998 research program by the MIT-ERL Reservoir Delineation Consortium. The focus is on displaying imaging results and evaluating the new vector image isochron (VII) imaging method.

The results are shown in two sections. First, images made with the imaging method of Miller et al. (1987), which is referred to as the conventional method, are shown. Issues such as fold correction, the resolution of the array, aperture limitation, and the difference between using 1D and 3D earth models for the traveltime calculation are addressed.

The conventional images are compared to previous results from the Michigan test site, showing that the downhole source, array geometry, and processing scheme of the 1998 MIT-ERL research program have combined to produce images of unprecedented resolution for this region of northern Michigan. However, array artifacts make the images difficult to interpret.

This leads to the second set of results: images made with the new (VII) imaging scheme, which are compared to their GRT migration counterparts. Although there is some cost in resolution, images made with VII migration show better continuity along reflectors and indicate clearly which structures are illuminated, allowing for more dependable interpretations.

4.1 Conventional migration results

The map on Figure 18 shows the location of the image slices are shown relative to the approximate position of the reef. The focus will be on the three north-south slices, since the array is very narrow in the east-west direction and resolution is poor on those slices. Before discussing issues related to the migration method, structural details of the imaged portion of the test site should be identified.

4.1.1 Geologic interpretation

Figure 19 is a velocity model of the structure of the reef and surrounding layers deduced from previous studies. The separation of the reef into two parts is due to a channel which was seen in a 1984 surface seismic study. No other studies have clearly indicated the presence of this channel; its presence is considered hypoythetical. Fine details, such as the pinchout of an anhydrite between the A2 salt and the A2 carbonate, are based on the fact that the A2 salt is present in off reef well logs but absent over the reef. The exact details of the pinch out are hypothesized.

Several interfaces are marked at the right edge of the middle slice: Event A at 4200 feet is carbonate stringers in a shale. Event B is the most obvious indicator of the presence of the reef: it is the interface between the B salt and the A2 carbonate which overlies the reef, stepping down off the reef to the north. The bottom of the reef E, which isn't expected to be a strong reflector, is at about 5000 feet. All events beneath the reef bottom are expected to be flat, such as the top of the Cabot Head shale marked F.

Events C and D are the tops of the A2 salt and the A1 anhydrite, which are high velocity contrasts in the off reef structure and pinch out over the reef. The A1 anhydrite has been conjectured to extend laterally into the reef (Jodry, 1969). If it does, it could be a barrier in fluid flow, trapping hydrocarbons in pockets within the reef.

Events A through E will be marked in all the figures in this chapter, and allow for comparison between the results of the different imaging schemes.

Figure 20 is a image formed by conventional Kirchhoff migration of the 1998 RVSP field data with a 15^o aperture limitation (the aperture limit is imposed on the dip of the imaged plane) and traveltimes calculated in the 3D earth model. There is a general trend in the image for events to dip upward at the edges: this is due to the limited nature of the imaging arrays. These "smiles" can be followed through the image, interfering with what are known to be flat reflectors, making detailed interpretation difficult.

The shallow reflectors, such as Event A, are flat and fairly even. Event F, however, shows an interruption at about -300 feet distance, which is likely due to an artifact from a deeper reflector.

The location of the reef can be clearly seen in the step of event B, but the reef bottom is not visible. Events C and D appear to dip downward into the reef, and appear to extend as far into the reef as the array can illuminate, or least until the upcurving artifactrs at the southern (left) edge of the image interfere.

No images previously produced at Michigan Test Site have had high enough resolution in 3D to pick up a detail like the extent of the A salt, Event C.

4.1.2 The Fold correction

Figure 21 shows vertical north-south slices of the fold of the survey, found by ray tracing through a flat layered earth model. This fold map can be used to even out the brightness of the reflectors in the image by dividing the image by the fold map. Portions of the image with low fold, less than 10 reflections per 25x25 foot (8x8 meter) bin, are cropped.

Figure 22 is a medium aperture conventional migration image of the reef, without the fold correction. Compared to Figure 20, which is the same image with the fold correction applied, the shallowest reflectors show the most obvious difference. They are evened out and can be followed further from the wellbore when the correction has been applied. The illumination of the deep reflectors are less uneven to begin with, thus they are less affected by the correction.

Unless otherwise stated, all conventional migration images discussed here will have the fold correction applied.

4.1.3 Aperture limitations

Figures 23 through 24 are north-south (NS) slices of images made by conventional Kirchhoff summation migration of the Michigan RVSP data, with traveltimes found in a flat layered earth. The three figures were made with aperture limits of 30^o, 15^o, and 5^o.

Figure 23 has a wide migration aperture of 30^o, and migration artifacts ("smiles") are a problem. The edges of the image are dominated by up-curving events. These events are suspiciously similar to the artifacts seen in the synthetic examples in the previous section, artifacts which were found to be directly caused by the borehole array geometry and the assumptions made in GRT migration.

The image in Figure 24 was created with a narrow migration aperture of 5^o. Event F shows more continuity than in the previous images, since the narrow aperture prevents energy from deeper reflectors from interfering. In general, reflection events appear fairly flat in this image, except in the furthest west slice, at -180 feet EW, which has a step in event B and a clearly downsloping event C.

Despite their high resolution, the GRT images are difficult to interpret because of the incompleteness of the receiver array. Even the central portion of the image with the highest fold shows artifacts which interfere with reflectors which are known to be flat.

4.2 Results with the VII method

Figures 25 and 26 show north-south slices of the image, without and with the fold correction. The images were formed by migrating all the data into a vector image, then transforming once for an average value of source depth.

In general, all reflectors have lost sharpness. This is an unfortunate effect of the VII transform: it inherently involves running a mean filter over the image. Also, strong reflectors, such as the reef top and

Event F, have become brigh. This makes it more difficult to see dim reflectors, such as those between Events E and F, in the "wiggle" trace display.

Event A and all the reflectors above the reef are not as flat as they were in the conventional migration image. This portion of the image grid is actually above some of the shot points, as the borehole array extends to 4500 feet and the top of the image grid is 4000 feet. For this reason, the shallow reflectors are the most prone to error caused by the constant velocity earth assumption made in the derivation of the vector image isochrons.

Event C is slightly flatter in the VII image than it was in the GRT image. Event E fades out and begins to curl up at the western (left) edge of the image, suggesting that this is the limit of the illumination of the array. It seems likely then that Event C also extends into the reef, at least as far as the array can illuminate.

Event F in the deepest part of the image is now a single flat reflector, not broken up by artifacts from deeper reflectors as it was in the conventional migration images.

The fold correction has a similar effect as in the conventional migration images, making the reflectors easier to follow to the edges of the image grid, and providing a way of knowing where to crop the image.

5 Conclusions

This research presents a new option for dealing with artifacts caused by limited aperture arrays. Current methods of removing these artifacts diminish dipping reflectors, reducing the usefulness of the image.

The imaging scheme presented in this paper, vector image isochron (VII) migration, can minimize artifacts in images created with limited aperture arrays. Images made with VII migration show more continuity along reflectors than images made with the conventional method, without the loss of energy on dipping reflectors.

The VII method reduces the resolution of the image slightly because it inherently involves running a mean filter over the image. Therefore, this scheme should be only be used when the array aperture is limited enough to cause problems in the image.

There are currently two limitations to the method. First, the derivation of the vector image isochrons is ray-based, so an explicit solution for any general earth model is not possible. This research assumes a constant velocity earth in the derivation, which causes error in portions of the image grid which are the shallowest and furthest out from the shot, and involve the most ray curvature. Second, the transform of borehole seismic data assumes that the shot depth is fixed. This requires that the data be migrated and transformed one shot at a time, a time consuming process. However, in many cases a mean value of shot depth can be used to transform the entire image. This is a good estimation when the image grid is deeper than the shots.

References

J. Gazdag. Wave equation migration with the phase shift method. *Geophysics*, 43:1342–1351, 1978.

R. L. Jodry. Growth and dolomitization of Silurian reefs, St. Clair County, Michigan. *Bull. of the Amer. Assoc. of Petr. Geol.*, 53:957–981, 1969.

D. Miller, M. Oristaglio, and G. Beylkin. A new slant on seismic imaging: Migration and integral geometry. *Geophysics*, 52:943–964, 1987.

R. H. Stolt. Migration by Fourier transform. *Geophysics*, 43:23–48, 1978.

K. D. Wyatt and S. B. Wyatt. The Determination of subsurface structure information using a Vertical Seismic Profile. In *51st Ann. Internat. Mtg., Soc. Expl. Geophys., Expanded Abstracts*, pages 1915–1949, 1981.

A Surface seismic array isochrons

A.1 The isochron principle

Images made with surface seismic data tend to not have the kind of artifacts which the vector image isochron (VII) transform is designed to minimize. However, it is useful to derive the vector image isochrons for surface seismic arrays for completeness and to illustrate the process.

As described in Section 2.2, isochron curves are derived by equating two traveltimes, illustrated in Figure 3. First, the *migration traveltime* is the traveltime of rays which reflect off each plane in the image space. For surface seismics, there are several traveltimes for each imaged plane, as there are several scattering angles. At the image location $\mathbf{x}$ in Figure 3, the imaged plane orientation ϕ, and a specified incidence angle ι, define a source receiver pair and a migration traveltime. This is true of every $(\mathbf{x}, \phi)$ point in the image space, and is purely a mathematical construct. It does not necessarily correspond to a physical reflector.

The second traveltime in the equality is the *specular traveltime*, and involves assuming that a certain plane, such as the one described by an angle θ at point $\mathbf{x_{ref}}$ in Figure 3, is an actual reflector. Therefore, the data recorded by the source receiver pair will contain reflected energy at a traveltime which is dependent on the source and receiver positions and the reflector parameters $\mathbf{x_{ref}}$ and θ. If the traveltime along the migration raypath equals the time along the specular ray path for any source-receiver pair, $\mathbf{x_{ref}}$ and $\mathbf{x}$ will lie on an isochron in the vector image, and the migrated image at the point $\mathbf{x}$ will contain energy from the reflector at $\mathbf{x_{ref}}$.

The derivation of the isochrons starts by setting up the geometry of the reflected ray at the imaged plane, which defines the source and receiver location and migration traveltime. Then the specular traveltime for that source-receiver pair is calculated, and finally the two times are set equal.

Since the isochrons depend on ray paths, they cannot be derived in a general earth model. The derivation presented here makes two assumptions; (1) a constant velocity earth, and (2) linear or, in 3D, planar reflectors. In the remainder of this section, expressions for the vector image isochrons will be derived for surface seismic arrays, in 2D and 3D. Section B derives vector image isochrons for borehole seismic arrays in 2D and 3D.

A.2 The geometry at the reflector

To describe the normal to the imaged plane $\mathbf{p}$ and the ray normals $\mathbf{s}$ and $\mathbf{r}$ in terms of the angles ι and θ, start in the coordinate system rotated so that the z' axis is in the direction of the $\mathbf{p}$. In the prime coordinate system, as shown in Figure 2,

$$\begin{aligned} \mathbf{p}' &= [0, 0, 1] \\ \mathbf{s}' &= [-\cos\iota_a \sin\iota_d, \quad -\sin\iota_a \sin\iota_d, \quad \cos\iota_d] \\ \mathbf{r}' &= [\cos\iota_a \sin\iota_d, \quad \sin\iota_a \sin\iota_d, \quad \cos\iota_d] \end{aligned} \tag{A-1}$$

These normals are rotated according to the imaged plane orientation. First, around the y axis by the imaged plane dip angle ϕ_d, then around the z axis by the imaged plane azimuth angle ϕ_a:

$$R_{zy} = R_z R_y = \begin{bmatrix} \cos\phi_a & -\sin\phi_a & 0 \\ \sin\phi_a & \cos\phi_a & 0 \\ 0 & 0 & 1 \end{bmatrix} * \begin{bmatrix} \cos\phi_d & 0 & \sin\phi_d \\ 0 & 1 & 0 \\ -\sin\phi_d & 0 & \cos\phi_d \end{bmatrix} \tag{A-2}$$

The resulting normals are:

$$\mathbf{p} = \mathbf{R}\mathbf{p}' = [\cos\phi_{\mathbf{a}} \sin\phi_{\mathbf{d}}, \sin\phi_{\mathbf{a}} \sin\phi_{\mathbf{d}}, \cos\phi_{\mathbf{d}}] \tag{A-3}$$

$$\begin{aligned} \mathbf{s} &= R\mathbf{s}' \\ &= \begin{bmatrix} -\cos\iota_a \sin\iota_d \cos\phi_a \cos\phi_d + \sin\iota_a \sin\iota_d \sin\phi_a + \cos\iota_d \cos\phi_a \sin\phi_d \\ -\cos\iota_a \sin\iota_d \sin\phi_a \cos\phi_d - \sin\iota_a \sin\iota_d \cos\phi_a + \cos\iota_d \sin\phi_a \sin\phi_d \\ \cos\iota_a \sin\iota_d \sin\phi_d + \cos\iota_d \cos\phi_d \end{bmatrix} \end{aligned} \tag{A-4}$$

$$\begin{aligned}\mathbf{r} &= R\mathbf{r}' \\ &= \begin{bmatrix} \cos\iota_a \sin\iota_d \cos\phi_a \cos\phi_d - \sin\iota_a \sin\iota_d \sin\phi_a + \cos\iota_d \cos\phi_a \sin\phi_d \\ \cos\iota_a \sin\iota_d \sin\phi_a \cos\phi_d + \sin\iota_a \sin\iota_d \cos\phi_a + \cos\iota_d \sin\phi_a \sin\phi_d \\ -\cos\iota_a \sin\iota_d \sin\phi_d + \cos\iota_d \cos\phi_d \end{bmatrix}\end{aligned} \tag{A-5}$$

In a constant velocity earth, the raypaths are straight and the source and receiver locations can be calculated from the image point $\mathbf{x}$ and the ray normals $\mathbf{s}$ and $\mathbf{r}$:

$$\mathbf{x} = [x, y, z] \tag{A-6}$$

$$\mathbf{x_s} = \mathbf{x} + (z_s - z)\frac{\mathbf{s}}{s_3} \tag{A-7}$$

$$\mathbf{x_r} = \mathbf{x} + (z_r - z)\frac{\mathbf{r}}{r_3} \tag{A-8}$$

where s_3 and r_3 are the z components of $\mathbf{s}$ and $\mathbf{r}$. The z components of $\mathbf{s}$ and $\mathbf{r}$ give the angle of the ray from the vertical, which leads to the migration ray path length as a function of the image point depth, the imaged plane dip, and the incidence angle:

$$\begin{aligned} s_{mig} &= \frac{z}{s_3} + \frac{z}{r_3} \\ &= \frac{2z\cos\iota_d \cos\phi_d}{\cos\iota_d{}^2 \cos\phi_d{}^2 - \cos\iota_a{}^2 \sin\iota_d{}^2 \sin\phi_d{}^2} \end{aligned} \tag{A-9}$$

The specular traveltime is found by adapting a 2D VSP formula from Wyatt and Wyatt (1981), although the notation used in this paper is reverse VSP. Given a surface receiver at $(x_r, 0)$, a downhole source at (x_s, z_s), and a planar reflector described by its dip angle θ_d and its depth d at the source x location, the ray path length of the specular ray in a constant velocity earth is:

$$\begin{aligned} s_{sr}^2 = (x_s - x_r)^2 + z_s^2 + 4d(d - z_s)\cos\theta_d{}^2 \\ +4(x_s - x_r)(d - z_s)\sin\theta_d \cos\theta_d \end{aligned} \tag{A-10}$$

Section C uses a coordinate rotation to apply Equation A-10 to the 3D case when θ is vector valued, the receiver is at $(x_r, y_r, 0)$, and the source is at $(x_s, y_s, 0)$:

$$\begin{aligned} s_{sr}^2 = ((x_r - x_s)\cos\theta_a + (y_r - y_s)\sin\theta_a{}^2 + z_s^2 + 4d^2\cos\theta_d{}^2 \\ +4(z_s - d)((x_r - x_s)\cos\theta_a + (y_r - y_s)\sin\theta_a)\sin\theta_d \cos\theta_d \end{aligned} \tag{A-11}$$

At this point, the derivation is continued in 2D. Examination of the results in 2D leads to a simplification which is used in the derivation of 3D surface seismic array isochrons.

A.3 Surface seismic isochrons in 2D

To reduce the problem to two dimensions, take $\phi_a = \iota_a = 0$. Equations A-3, A-4 and A-5 become:

$$\mathbf{p} = [\sin\phi_d, 0, \cos\phi_d], \tag{A-12}$$

$$\mathbf{s} = [-\sin\iota_d \cos\phi_d + \cos\iota_d \sin\phi_d, 0, \sin\iota_d \sin\phi_d + \cos\iota_d \cos\phi_d] \tag{A-13}$$

$$\mathbf{r} = [\sin\iota_d \cos\phi_d + \cos\iota_d \sin\phi_d, 0, -\sin\iota_d \sin\phi_d + \cos\iota_d \cos\phi_d] \tag{A-14}$$

Equations A-6, A-7, and A-8 with $z_s = z_r = 0$, become:

$$\mathbf{x} = [x, 0, z] \tag{A-15}$$

$$\begin{aligned}\mathbf{x_s} - \mathbf{x} &= -z\frac{\mathbf{i}}{i_3} \\ &= [-z\tan\iota_d + \theta_d, 0, -z] \qquad \text{(A-16)} \\ & \qquad\qquad\qquad\qquad\qquad\qquad\qquad\qquad\qquad\qquad\qquad\qquad \text{(A-17)}\end{aligned}$$

$$\begin{aligned}\mathbf{x_r} - \mathbf{x} &= -z\frac{\mathbf{r}}{r_3} \\ &= [-z\tan\iota_d - \theta_d, 0, -z] \qquad \text{(A-18)}\end{aligned}$$

From Eq. A-10, the migration ray path length with $\theta_a = 0$ is:

$$\begin{aligned}s_{mig} &= 2z\frac{\cos\iota_d\cos\theta_d}{\cos{\iota_d}^2 - \sin{\theta_d}^2} \\ &= z\left(\frac{1}{(\cos\iota_d + \theta_d)} + \frac{1}{(\cos\iota_d - \theta_d)}\right) \qquad \text{(A-19)}\end{aligned}$$

Since the velocity is constant, the ray paths length can be equated instead of traveltimes. Using the ray path length Equation A-10, with the depth of the reflector at the source d, expressed in terms of the reflector depth at the image point z_{ref}, so $d = z_{ref} + (x_s - x)\tan\theta_d$:

$$\begin{aligned}s_{sr}^2 = (x_s - x_r)^2 + 4(z_{ref} + (x_s - x)\tan\theta_d)^2\cos{\theta_d}^2 \\ +4(x_s - x_r)(z_{ref} + (x_s - x)\tan\theta_d)\sin\theta_d\cos\theta_d \qquad \text{(A-20)}\end{aligned}$$

The source and receiver locations given in Equation A-16 and A-18 are plugged into A-20, giving an expression for the ray path distance squared as a function of z, ϕ_d, ι_d, z_{ref}, and θ_d. Since the source and receiver arrays are assumed to extend over the entire surface, the x position of the image point is taken to be the origin with no loss of generality.

The square root of Equation A-20 is equated to the migration raypath A-19

$$s_{sr}(z, \phi_d, \iota_d, z_{ref}, \theta_d) = s_{mig}(z, \phi_d, \iota_d) \qquad \text{(A-21)}$$

leading to a quadratic equation for z with the following solution:

$$\frac{z}{z_{ref}} = \frac{\cos\theta_d(\sin\theta_d\sin\phi_d\cos\phi_d \pm \cos\iota_d\sqrt{\cos{\phi_d}^2 - \cos{\theta_d}^2\sin{\iota_d}^2}}{\cos{\theta_d}^2\cos{\iota_d}^2 + \sin{\theta_d}^2\cos{\phi_d}^2} \qquad \text{(A-22)}$$

The roots of Equation A-22 are complex when $\sin{\phi_d}^2 > \cos{\iota_d}^2$. This corresponds to the case when at least one of the reflected or incident ray is downgoing, and so can't reach the surface.

A.4 Surface seismic isochrons in 3D

The example in 2D showed that the energy of reflected events in the surface seismic vector image lies predominantly along the $\iota_d = 0$ contour. It is possible to make contours in 3D for any value of ι_d, but it isn't necessary, and much troublesome algebra can be avoided by setting $\iota_d = 0$ initially. Therefore, $\mathbf{s}$ and $\mathbf{r}$ are equal to $\mathbf{p}$ and the source and receiver have the same location $\mathbf{x_s}$.

In 3D, the reflector is described by its depth z_{ref} at the image point and the orientation of its normal, a two valued angle $\theta = [\theta_a, \theta_d]$. The imaged plane is similarly described by a two valued vector $\phi = [\phi_a, \phi_d]$.

Equation A-11 gives the ray path length between a surface source and a surface receiver given a planar reflector. If $x_s = x_r$ and $y_s = y_r$:

$$s_{sr} = 2d\cos\theta_d \qquad \text{(A-23)}$$

where d is the depth of the reflector at the source location:

$$d = z_{ref} - x_s\cos\theta_a\tan\theta_d - y_s\sin\theta_a\tan\theta_d \qquad \text{(A-24)}$$

Equations A-23 and A-24 give a specular ray path length of:

$$s_{sr} = 2z_{ref}\cos\theta_d - 2\sin\theta_d(x_s\cos\theta_a + y_s\sin\theta_a) \tag{A-25}$$

This distance is evaluated at the source and receiver locations defined by the imaged plane:

$$\begin{aligned} x_s &= -z\cos\phi_a\tan\phi_d \\ y_s &= -z\sin\phi_a\tan\phi_d \end{aligned} \tag{A-26}$$

and set equal to the migration ray path length Equation A-9 with $\iota_d = 0$:

$$s_{mig} = \frac{2z}{\cos\phi_d} \tag{A-27}$$

with the result:

$$\frac{z}{z_{ref}} = \frac{-\cos\theta_d\cos\phi_d}{1+\sin\phi_d\sin\theta_d(\cos\phi_a\cos\theta_a + \sin\phi_a\sin\theta_a)} \tag{A-28}$$

In the 2D case where $\theta_a = \phi_a = 0$,

$$\frac{z}{z_{ref}} = \frac{-\cos\theta_d\cos\phi_d}{1+\sin\phi_d\sin\theta_d} \tag{A-29}$$

which, with some trig manipulation, is the same as the 2D result Equation A-22 with $\theta_d = 0$.

B Borehole seismic array isochrons

A different approach is needed to map isochrons in borehole seismic vector images, since the source array has a fixed (x, y) location, but varies in depth.

The approach taken here is to fix the source depth and to calculate the isochrons one shot depth at a time. (The consequences of this assumption will were discussed in Section 3.6.) Since the isochrons are mapped one shot depth at a time, there is only one raypath which illuminates each image point and plane. The incidence angle ι will not be an independent variable as it was in the case of surface seismic arrays.

Another difference between surface array and borehole array isochrons, caused by the fixed (x, y) location of the source, is that the shape of the isochrons will be different at different image (x, y) locations. Therefore, the origin is taken to be the shot location instead of the image location. The depth of the model reflector will still be measured at the origin, but now this will be at the source, and not at the image point.

B.1 Borehole seismic array isochrons in 2D

Figure 6 shows the geometry of the raypaths at the reflector. As mentioned above, this is different from the surface seismic case because the incident angle is determined by the imaged point and plane and the source location. Equations A-3 through A-9 from the surface seismic derivation still hold, but each imaged plane will have only one specular ray, and one corresponding value of ι.

The borehole seismic isochrons are found numerically by equating specular and migration ray path lengths according to Equation A-10 in 2D and Equation A-11 in 3D.

In 2D, an image point at $(x,\ z,\ \phi_d)$ and a reflector with dip angle θ_d and depth z_{ref} at the origin has migration and specular ray path lengths:

$$\begin{aligned} s_{mig}^2 = (x_s - x_r)^2 + z_s^2 + 4d(d - z_s)\cos{\phi_d}^2 \\ +4(x_s - x_r)(d - z_s)\sin\phi_d\cos\phi_d \end{aligned} \tag{B-1}$$

$$\begin{aligned} s_{sr}^2 = (x_s - x_r)^2 + z_s^2 + 4z_{ref}(z_{ref} - z_s)\cos{\theta_d}^2 \\ +4(x_s - x_r)(z_{ref} - z_s)\sin\theta_d\cos\theta_d \end{aligned} \tag{B-2}$$

where d is the depth of the imaged plane at the source x location:

$$d = z + (x - x_s)\tan\phi_d. \tag{B-3}$$

The source location (x_s, z_s) is fixed, and the receiver location x_r is found by solving for the incidence angle ι_d. Eq. A-16 can be rearranged:

$$\iota_d = \arctan\frac{x_s - x}{z_s - z} - \phi_d \tag{B-4}$$

leading to the receiver location.

$$x_r = x + z\frac{x - (z_s - z)\tan 2\phi_d}{z_s - z + x\tan 2\phi_d} \tag{B-5}$$

Setting the traveltimes in Eq. B-1 and B-2 equal:

$$\begin{aligned} &4d(d - z_s)\cos\phi_d{}^2 + 4(x_s - x_r)(d - z_s)\sin\phi_d\cos\phi_d \\ &= 4z_{ref}(z_{ref} - z_s)\cos\theta_d{}^2 + 4(x_s - x_r)(z_{ref} - z_s)\sin\theta_d\cos\theta_d \end{aligned} \tag{B-6}$$

which is solved numerically for z.

B.2 Borehole seismic array isochrons in 3D

In 3D, the same process is followed, with slightly more complicated expressions. The image point (x, y, z, ϕ_a, ϕ_d) and reflector with orientation $\theta = (\theta_a, \theta_d)$ and depth z_{ref} at the origin has ray path lengths:

$$\begin{aligned} s_{mig}^2 = {} & (x_r\cos\phi_a + y_r\sin\phi_a)^2 + z_s^2 - 4d(z_s - d)\cos\phi_d{}^2 \\ & +4(x_r\cos\phi_a + y_r\sin\phi_a)(z_s - d)\sin\phi_d\cos\phi_d \end{aligned} \tag{B-7}$$

$$\begin{aligned} s_{sr}^2 = {} & (x_r\cos\theta_a + y_r\sin\theta_a)^2 + z_s^2 - 4z_{ref}(z_s - z_{ref})\cos\theta_d{}^2 \\ & +4(x_r\cos\theta_a + y_r\sin\theta_a)(z_s - z_{ref})\sin\theta_d\cos\theta_d \end{aligned} \tag{B-8}$$

where d is the imaged plane depth at the source x location:

$$z_{ref} = z + (x - x_s)\cos\phi_a\tan\phi_d + (y - y_s)\sin\phi_a\tan\phi_d \tag{B-9}$$

The incidence angle is found by defining A_s and B_s from Equation A-4:

$$A_s = \frac{x_s - x}{z_s - z} = \frac{s_1}{s_3} \tag{B-10}$$

$$B_s = \frac{y_s - y}{z_s - z} = \frac{s_2}{s_3} \tag{B-11}$$

and solving for $\tan\iota_d$:

$$\begin{aligned} \tan\iota_d &= \frac{\cos\phi_a\sin\phi_d - A_s\cos\phi_d}{A_s\cos\iota_a\sin\phi_d + \cos\iota_a\cos\phi_a\cos\phi_d - \sin\iota_a\sin\phi_a} \\ \tan\iota_d &= \frac{\sin\phi_a\sin\phi_d - B_s\cos\phi_d}{B_s\cos\iota_a\sin\phi_d + \cos\iota_a\sin\phi_a\cos\phi_d + \sin\iota_a\cos\phi_a}. \end{aligned} \tag{B-12}$$

These are set equal to each other to solve for ι_a:

$$\begin{aligned} &\cos\iota_a(B_s\cos\phi_a - A_s\sin\phi_a) \\ &= \sin\iota_a(B_s\sin\phi_a\cos\phi_d + A_s\cos\phi_a\cos\phi_d - \sin\phi_d). \end{aligned} \tag{B-13}$$

The receiver position according to Equation A-8, with the receiver depth set to 0, is

$$\begin{aligned} x_r - x &= -z\frac{r_1}{r_3} \\ y_r - y &= -z\frac{r_2}{r_3} \end{aligned} \tag{B-14}$$

Equations B-12 and B-13 are used to eliminate ι_a and ι_d from r_1, r_2, and r_3 in Equation B-14. The results are expressions for x_r and y_r in terms of x, y, x_s, y_s, ϕ_a, and ϕ_d.

Equating the migration ray path length (Equation B-7) and the specular ray path length (Equation B-8) leads to an expression for the borehole seismic vector image isochrons. The solution, found numerically, describes a surface in depth z in terms of variables ϕ_a, and ϕ_d, with x, y, x_s, y_s, z_s, z_{ref}, θ_a and θ_d fixed.

C Derivation: an expression for ray path length in 3D

An expression is needed for the traveltime of a reflected ray in 3D given a constant velocity earth, a source location $\mathbf{x_s} = [x_s, y_s, z_s] = [0, 0, z_s]$, a receiver location $\mathbf{x_r} = [x_r, y_r, z_r] = [x_r, y_r, 0]$, and a planar reflector described by its depth at the origin d the azimuth θ_a and dip θ_d of its normal.

This problem is solved in a rotated coordinate system where the reflector is flat, so that the source, receiver and image point are all in the same vertical plane. Then the expression A-10 from Wyatt and Wyatt (1981) is applied.

The rotation into the prime coordinate system where the reflector is flat is given in Equation A-2. The inverse rotation is

$$R'_{zy} = R'_z R'_y = \begin{bmatrix} \cos\phi_d & 0 & -\sin\phi_d \\ 0 & 1 & 0 \\ \sin\phi_d & 0 & \cos\phi_d \end{bmatrix} * \begin{bmatrix} \cos\phi_a & \sin\phi_a & 0 \\ -\sin\phi_a & \cos\phi_a & 0 \\ 0 & 0 & 1 \end{bmatrix} \tag{C-1}$$

In the prime coordinate system, the source and receiver coordinates are:

$$x'_r = R'[x_r, y_r, 0] \tag{C-2}$$

$$= \begin{bmatrix} (x_r\cos\theta_a + y_r\sin\theta_a)\cos\theta_d \\ -x_r\sin\theta_a + y_r\cos\theta_a \\ (x_r\cos\theta_a + y_r\sin\theta_a)\sin\theta_d \end{bmatrix} \tag{C-3}$$

$$x'_s = R'[0, 0, z_s] = [-z_s\sin\theta_d, 0, z_s\cos\theta_d] \tag{C-4}$$

The depth of the reflector in the primed coordinate system is:

$$\begin{aligned} d' &= R'(d - x\cos\theta_a\tan\theta_d - y\sin\theta_a\tan\theta_d) \\ &= d\cos\theta_d \end{aligned} \tag{C-5}$$

In the prime coordinate system the reflector has zero dip, and since the source is at the x, y origin, $z'_s = z_s$, and the distance formula Eq. A-10 becomes:

$$s^2_{sr} = (x'_s - x'_r)^2 + z^2_s + 4d'_o(d'_o - z_s) \tag{C-6}$$

Plugging Eq. C-2 and Eq. C-4 into Eq. C-6:

$$\begin{aligned} s^2_{sr} = &((x_r - x_s)\cos\theta_a + (y_r - y_s)\sin\theta_a{}^2 + z^2_s + 4d^2\cos\theta_d{}^2 \\ &+4(z_s - d)((x_r - x_s)\cos\theta_a + (y_r - y_s)\sin\theta_a)\sin\theta_d\cos\theta_d \end{aligned} \tag{C-7}$$

If the azimuth angles are set to zero, Eq. C-7 equals the 2D expression Eq. A-10.

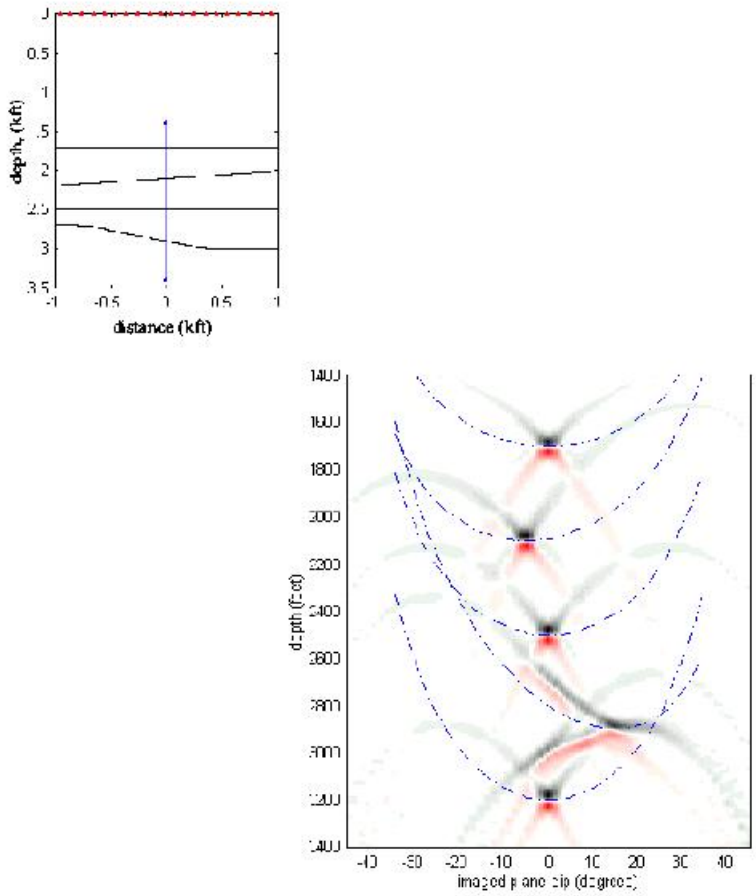

Figure 15: Transformed vector image from Figure 14 The final image was shown in Figure 16.

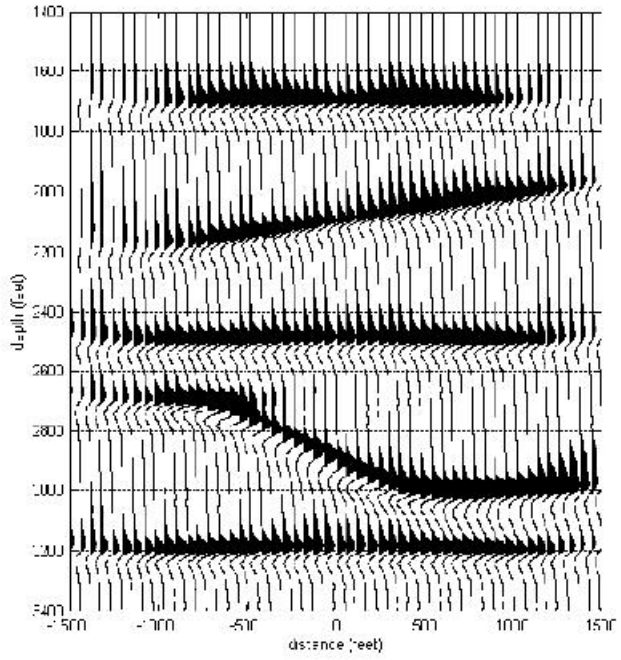

Figure 16: Image from the new imaging technique.

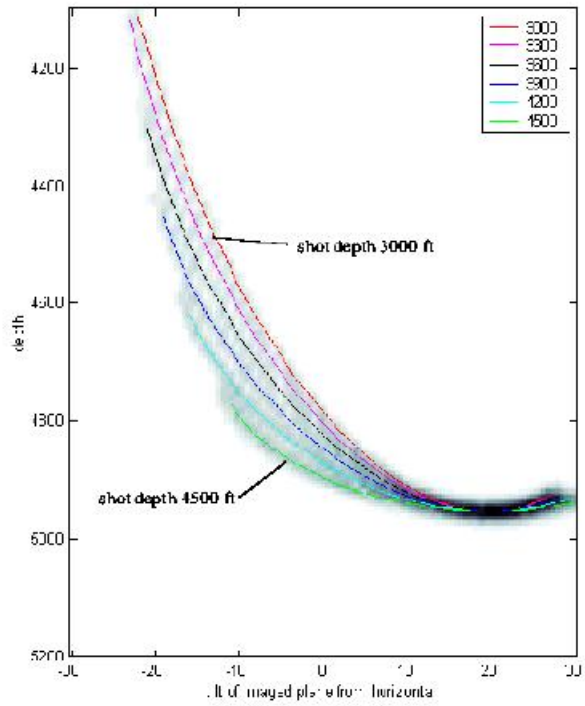

Figure 17: Vector image from synthetic 2D borehole seismic data, in grayscale. The overlain curves are vector image isochrons for different shot depths.

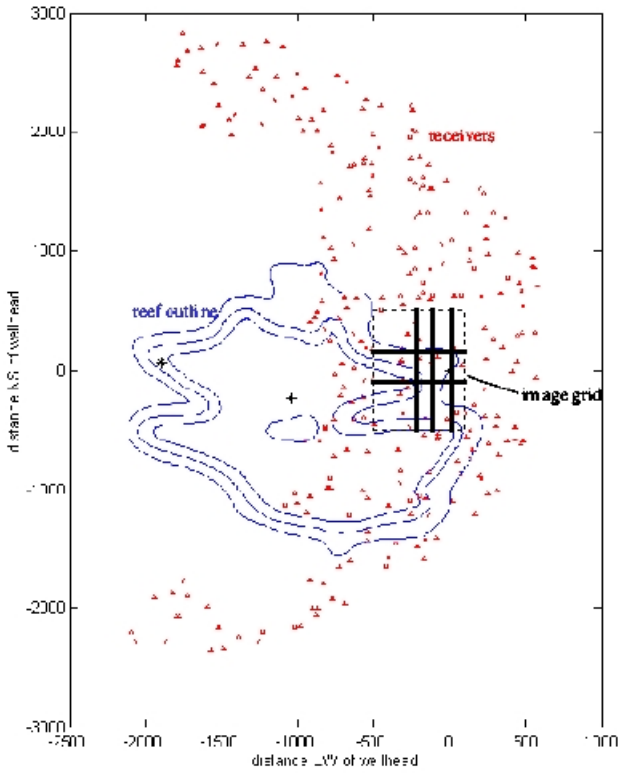

Figure 18: Location of image slices, shown in heavy black.

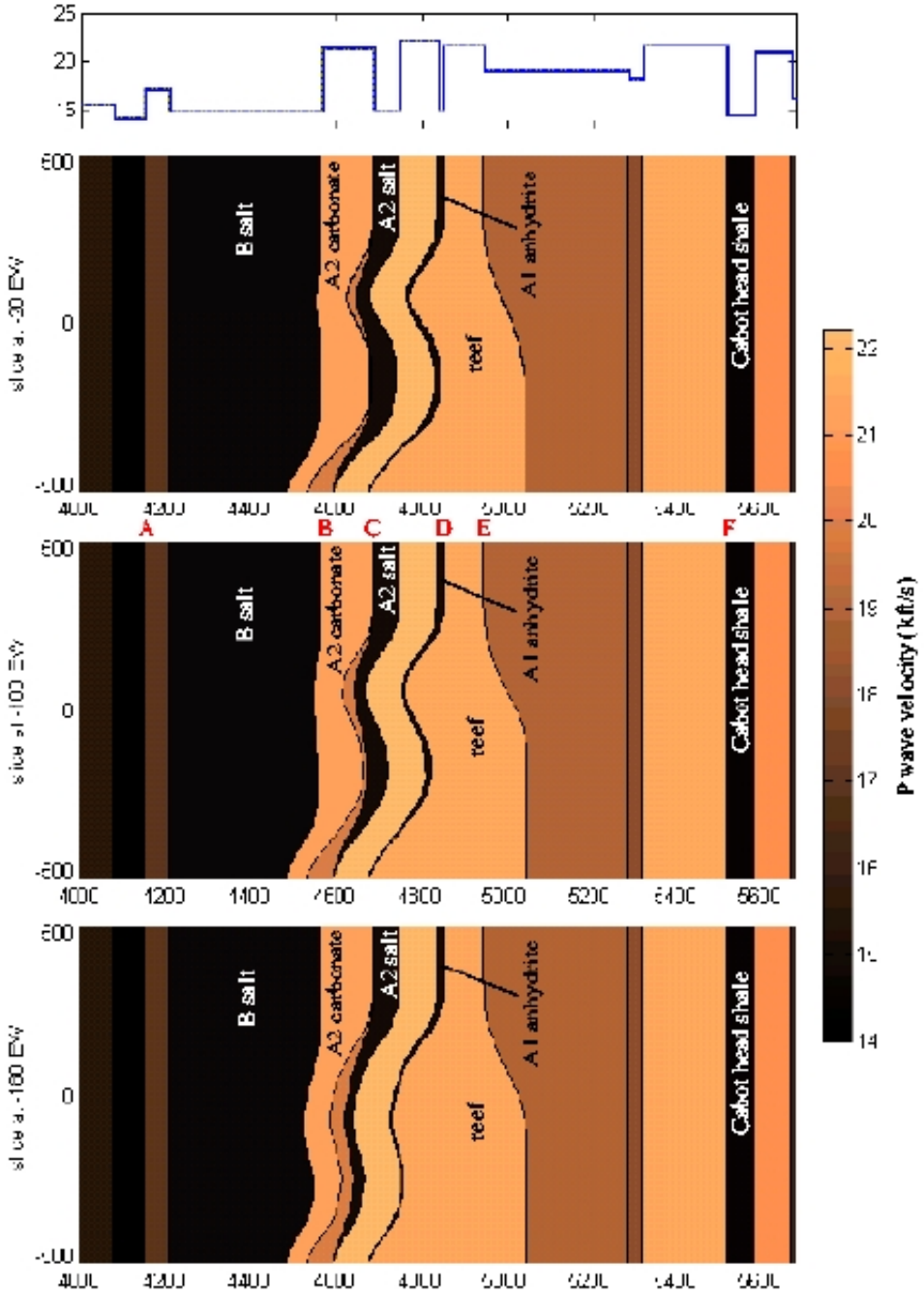

Figure 19: Earth structure from well logs and previous studies.

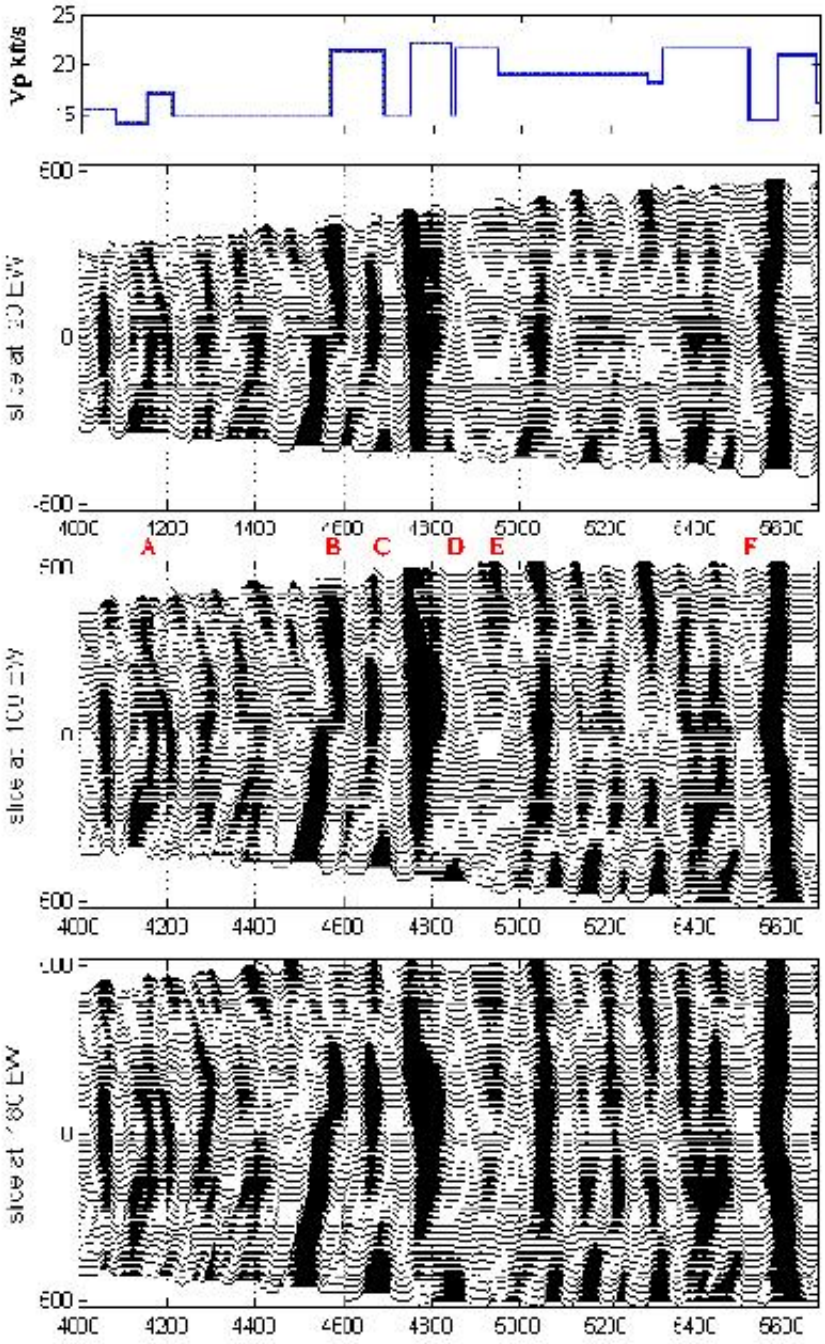

Figure 20: Medium aperture(15^o) conventional migration image with the 3D velocity model.

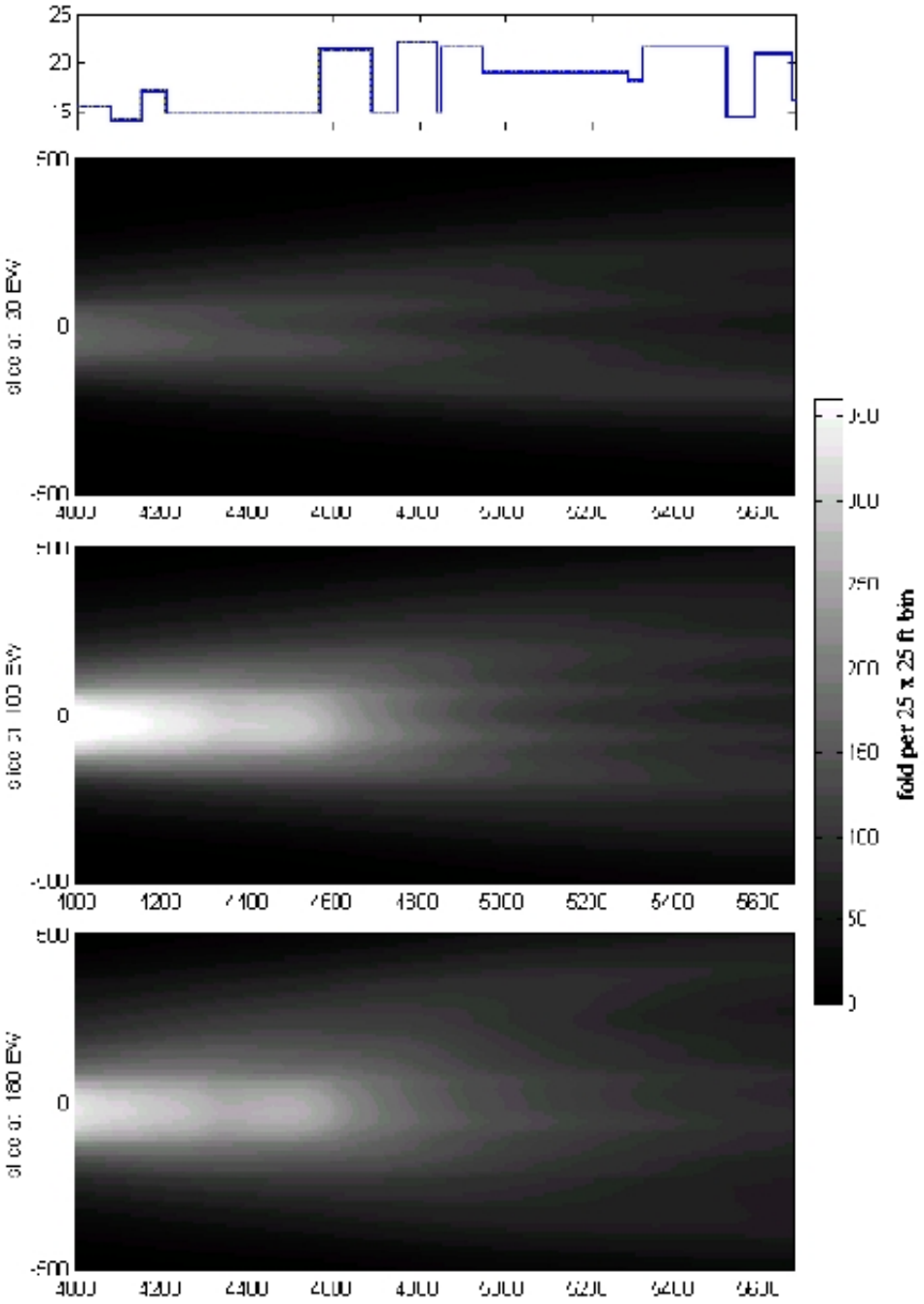

Figure 21: Fold map used for array illumination correction.

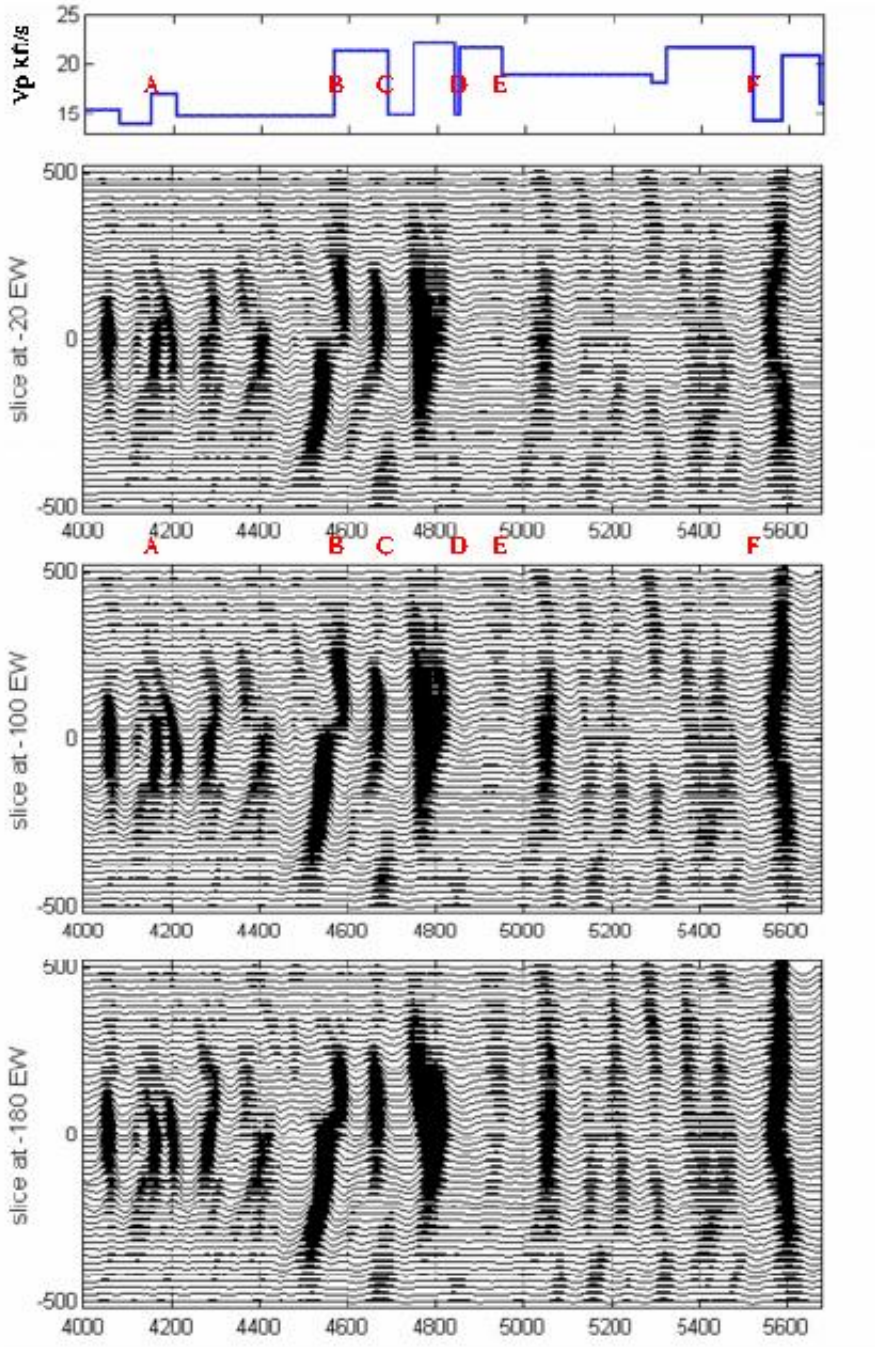

Figure 22: Image from Figure 20 without the fold correction.

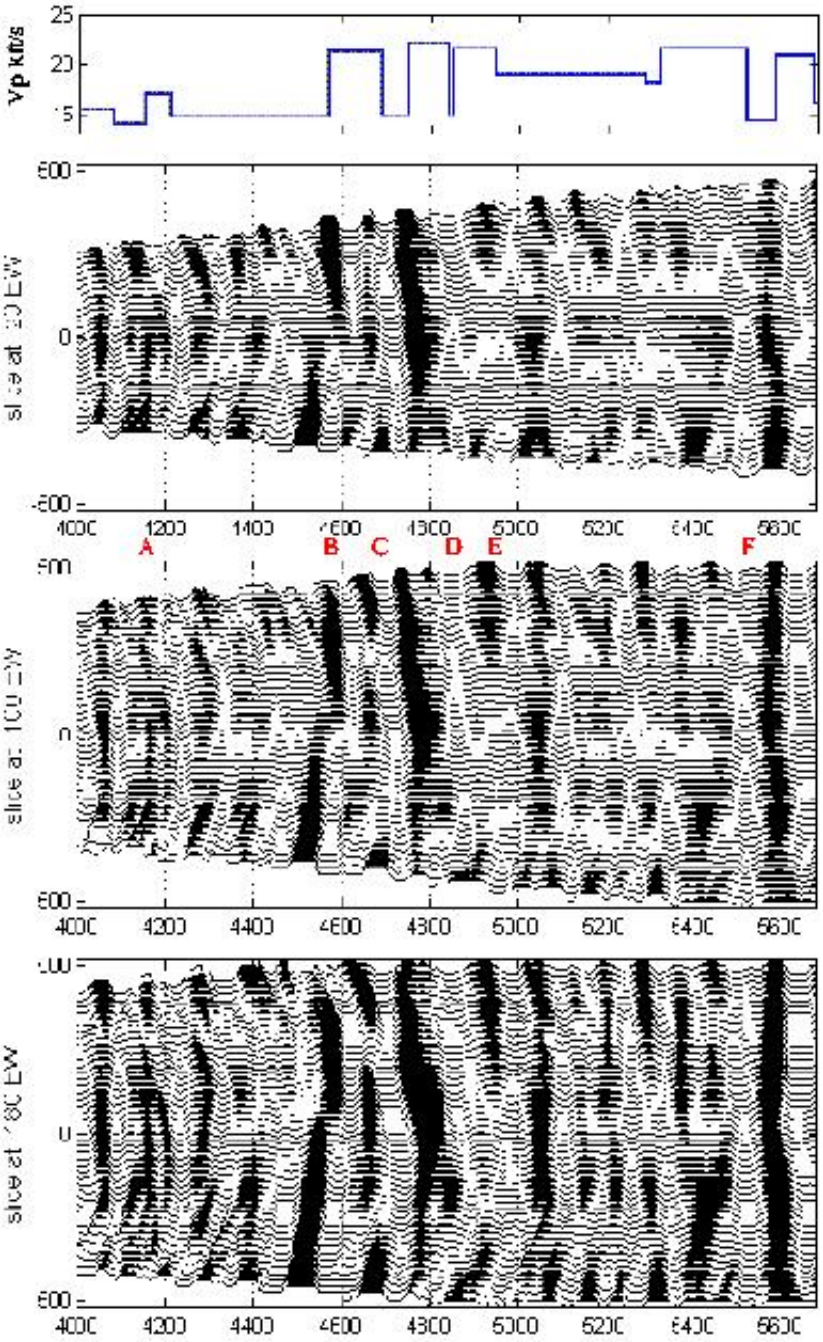

Figure 23: Wide aperture (30^o) GRT migration image.

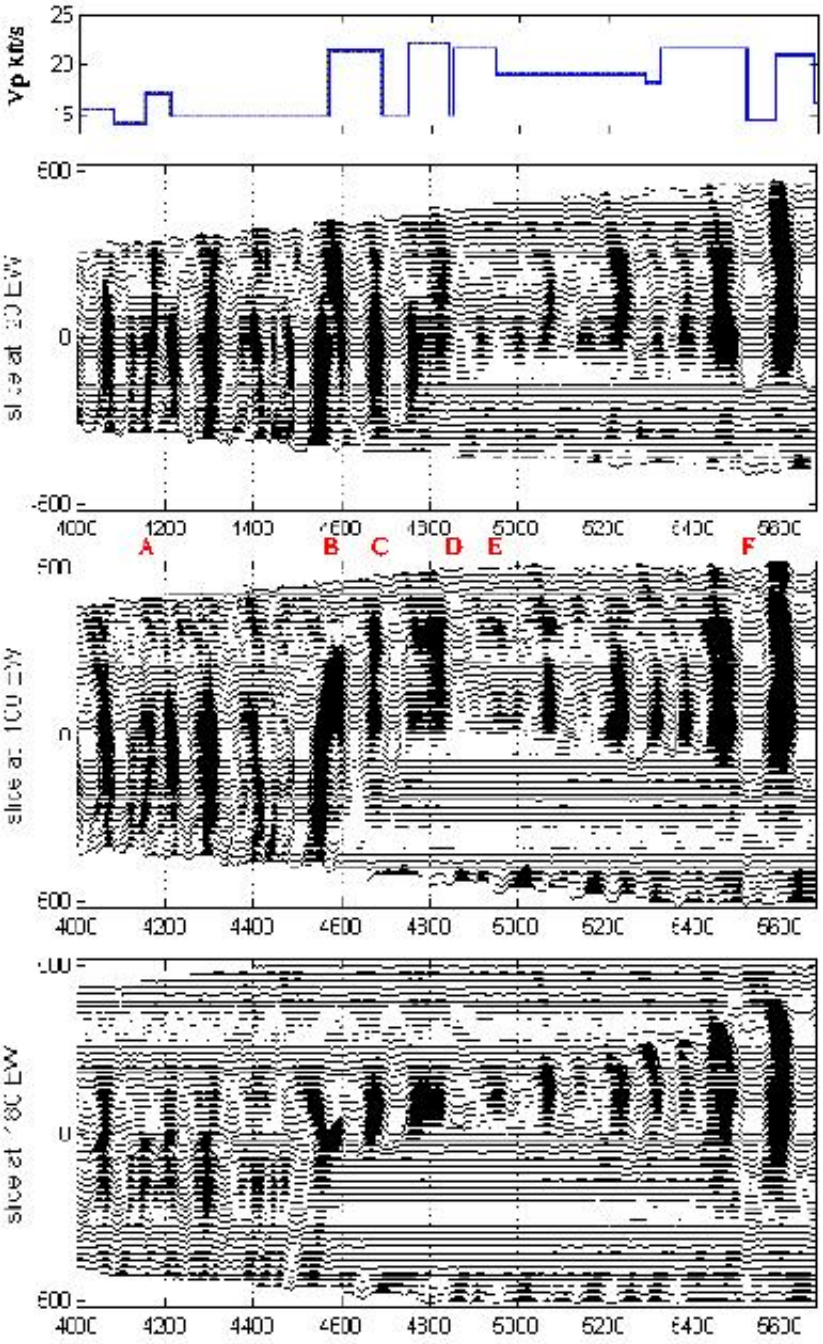

Figure 24: Narrow aperture (5°) GRT migration image.

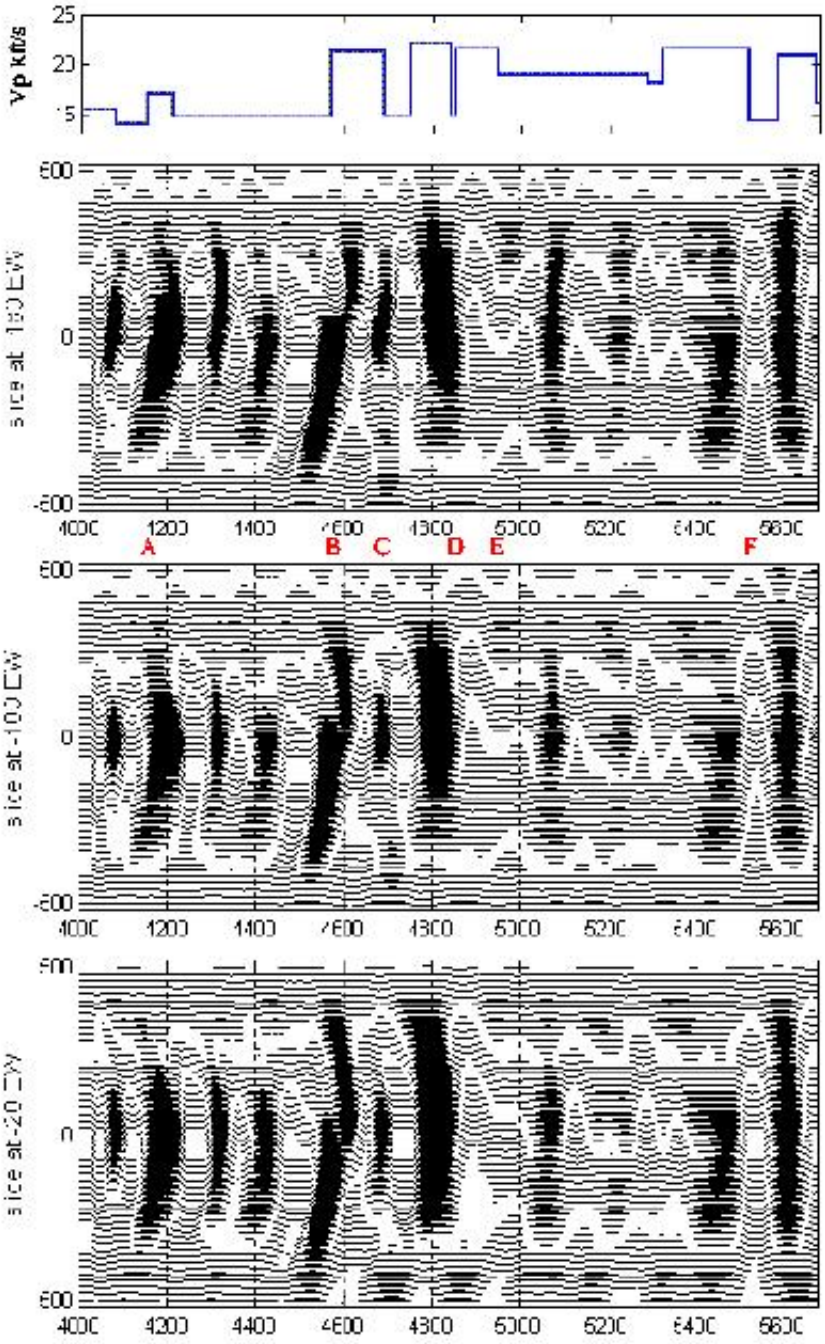

Figure 25: VII image with no fold correction.

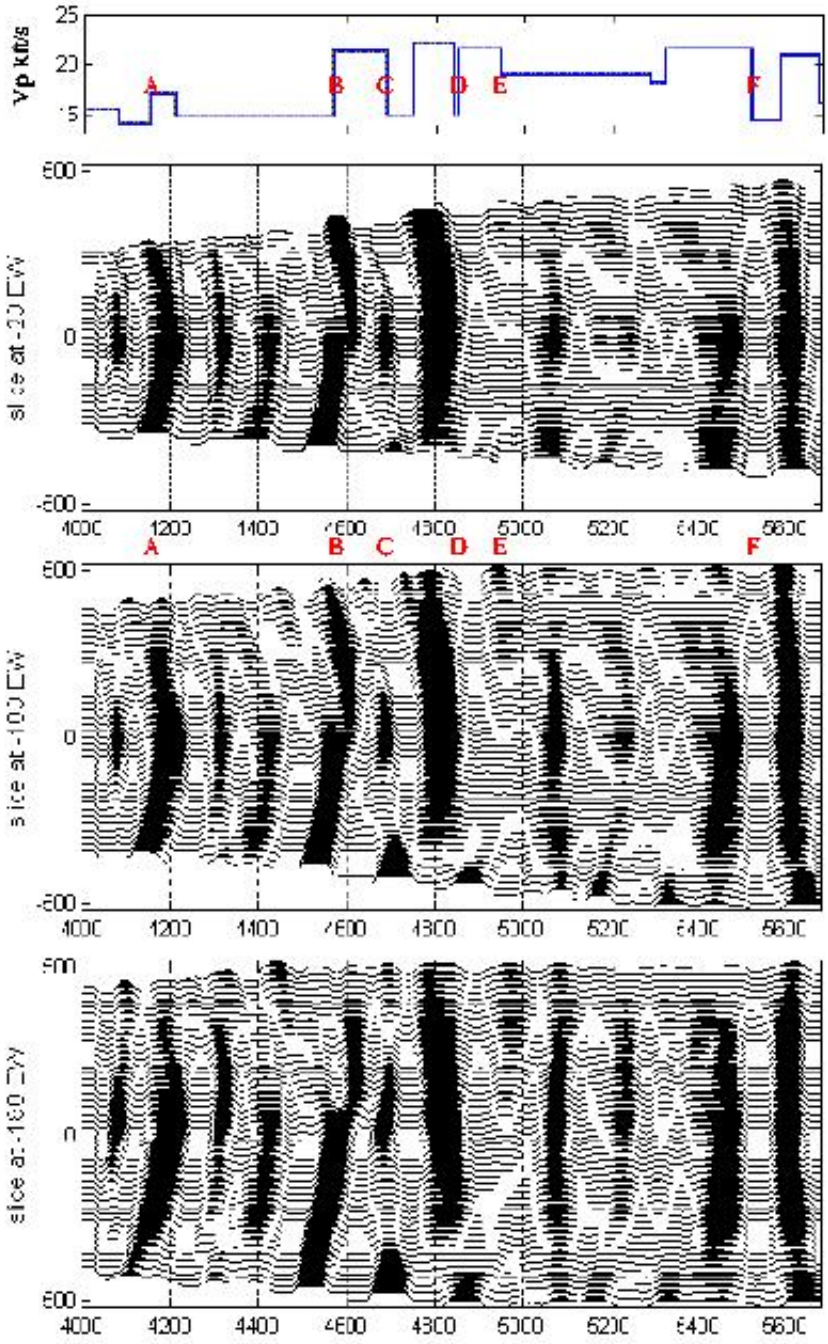

Figure 26: VII image with fold correction applied.